



139  
988  
THS



**PLACE IN RETURN BOX** to remove this checkout from your record.  
**TO AVOID FINES** return on or before date due.  
**MAY BE RECALLED** with earlier due date if requested.

<b>DATE DUE</b>	<b>DATE DUE</b>	<b>DATE DUE</b>

**DETERMINATION OF NOREPINEPHRINE IN RAT TISSUE BY REVERSED-  
PHASE HPLC SEPARATION AND AMPEROMETRIC DETECTION USING A  
BORON DOPED NANOCRYSTALLINE THIN FILM ELECTRODE**

**By**

**Luther Sterling Schaeffer**

**A THESIS**

**Submitted to  
Michigan State University  
In partial fulfillment of the requirements  
for the degree of**

**MASTER OF SCIENCE**

**Department of Chemistry**

**2006**

## ABSTRACT

### DETERMINATION OF NOREPINEPHRINE IN RAT TISSUE BY REVERSED-PHASE HPLC SEPARATION AND AMPEROMETRIC DETECTION USING A BORON DOPED NANOCRYSTALLINE THIN FILM ELECTRODE

By

Luther Sterling Schaeffer

The research presented herein describes the development and optimization of a reversed-phase high-performance liquid chromatography technique coupled with electrochemical detection (RP-HPLC-EC) for the analysis of catecholamines. The method relies on the beneficial electrochemical properties of a novel electrode material, boron-doped diamond. Detection of norepinephrine (NE), epinephrine (EP), dopamine (DA), 3,4-dihydroxyphenylethylene glycol (DOPEG), vanillic mandelic acid (VMA), normetanephrine (NM) and metanephrine (MN) was successfully performed with limits of detection (LOQ, S/N = 3) ranging from 245 pg to 3 ng. The method was applied to the quantitation of NE in rat tissues using a solid-phase extraction (SPE) technique for sample clean-up. The electrode response exhibited no signs of fouling after 80 days (RSD = 6.7 %), 100's of injections of tissue samples and required no rigorous pretreatment. The mechanism of catecholamine redox chemistry at diamond was also studied by cyclic voltammetry as a function of potential sweep rate and solution pH.

## ACKNOWLEDGEMENTS

Two and a half years I have visited Michigan.  
I was pushed until I believed I would fail yet somehow worked my way through.

Greg Swain, the Leader. You have pushed me harder and demanded more from me than anyone thus far. Thanks for the support, kicking me in the pants, and making this possible. Most of all, thank you for putting up with my indecisiveness.

Veronika Quaiserova-Mocko, my  $\beta$ -advisor and experimental muse. For guiding me, teaching me, and connecting all the dots...

Martin Novotny, CE-master. For the late night help with the wine boxes, the absinthe (thank you Dasa) and slivovice. Oh yea, and the method development too...

You were both instrumental in the success of this project and would like everyone to know of your significance. THANK YOU.

*At MSU...* I have learned and experienced chemistry, what it is to be a graduate student and met many people whom I now consider friends and family.

*In Lansing...* I have had many adventures and misadventures, discovered the subculture of the area and was welcomed into the community by great and unforgettable people.

Without all of these friends I would have drowned. Everyone, whom I have had the opportunity to meet, work with, unwind with, were all paramount in my development and success. Many thanks to you.

And finally, my Family, for listening to me over the while and tolerating my unrelenting pessimism and lapses of contact.

## TABLE OF CONTENTS

<b>List of Tables .....</b>	<b>vi</b>
<b>List of Figures.....</b>	<b>viii</b>
<b>Chapter 1: Introduction.....</b>	<b>1</b>
<b>Chapter 2: Experimental Methods.....</b>	<b>7</b>
Instrumental .....	7
2.1 Boron-Doped Diamond Thin Film Growth.....	7
2.2 Cyclic Voltammetry (CV).....	9
2.3 Reversed-Phase High Performance Liquid Chromatography .....	10
2.4 Thin-Layer Flow-Cell .....	11
Animals.....	13
2.5 Heart Tissue Preparation.....	13
2.6 Preparation of DOCA-salt Hypertensive and Sham Rat Models.....	14
2.7 Treatment with 6-OHDA .....	15
2.8 Tissue collection .....	16
2.9 Tissue sample homogenization .....	16
2.10 SPE Procedure.....	17
2.11 Materials and Chemicals .....	18
<b>Chapter 3: Cyclic Voltammetry of Norepinephrine at Boron-Doped Nanocrystalline and Microcrystalline Thin-Film Electrodes .....</b>	<b>20</b>
3.1 Introduction.....	20
3.2 Electrochemical Characterization of Diamond Electrodes .....	21
3.3 Cyclic Voltammetric Behavior of Norepinephrine.....	24
3.4 Measurement of NE Adsorption on BDD .....	39
<b>Chapter 4: Determination of Norepinephrine in Normal, Sham, DOCA-salt and 6-Hydroxydopamine Treated Rat Tissue by Reversed-Phase HPLC Separation and Amperometric Detection Using a Boron-Doped Nanocrystalline Diamond Thin-Film Electrode .....</b>	<b>43</b>
4.1 Introduction.....	43
4.2 Development of the Method for Neurogenic Amine Standards.....	46
4.3 Application of the HPLC-EC Method for the Quantitation of NE from Tissue.....	57
4.4 Preparation of Tissue for the Extraction of NE.....	59

4.5 Solid-Phase Extraction (SPE) of Tissue Supernatant.....	61
4.6 HPLC-EC Analysis of Tissue Extracts .....	66
4.6-1 Analysis of Various Tissue Extracts.....	67
4.6-2 Analysis of heart tissue and comparison of NE content in normotensive, DOCA-salt hypertensive, Sham, and 6-OHDA denervated models .....	73
4.7 Electrode Response Stability.....	78
<b>Chapter 5: Summary of Results and Conclusions .....</b>	<b>80</b>
5.1 Conclusions .....	80
<b>References .....</b>	<b>83</b>

## LIST OF TABLES

### **Chapter 3: Cyclic Voltammetry of Norepinephrine at Boron-Doped Nanocrystalline and Microcrystalline Thin-Film Electrodes**

Table 3.1. Comparison of experimentally observed and published values of  $\Delta E_p$  for  $\text{Fe}(\text{CN}_6)^{-3/-4}$  and  $\text{Ru}(\text{NH}_3)_6^{+2/+3}$ . Experimental values shown are the mean for 3 electrodes of each type along with the relative standard deviation.....24

Table 3.2. Experimental data recorded at BMD and BND for the  $\text{Fe}(\text{CN}_6)^{-3/-4}$  and  $\text{Ru}(\text{NH}_3)_6^{+2/+3}$  systems .....24

### **Chapter 4: Determination of Norepinephrine in Normal, Sham, DOCA-salt and 6-Hydroxydopamine Treated Rat Tissue by Reversed-Phase HPLC Separation and Amperometric Detection Using a Boron-Doped Nanocrystalline Diamond Thin-Film Electrode**

Table 4.1. Selected examples of mobile phase composition and column type for catecholamine analysis .....47

Table 4.2.  $E_{1/2}$  values obtained from hydrodynamic voltammograms for the solutes studied. Detection electrode = BND. Mobile phase was 50 mM ammonium formate buffer (pH3).....51

Table 4.3. Molecular structure, mass and  $pK_a$  values for catecholamines and related compounds .....52

Table 4.4. Figures of merit for the detection of catecholamines by the HPLC-EC system .....55

Table 4.5. Retention time and resolution for various catecholamines and metabolites .....56

Table 4.6. Average weight (n=2) of different heart chambers from the animal models used in this work .....58

Table 4.7. The volume of PCA to the tissue weight for various tissue types analyzed by HPLC-EC.....60

Table 4.8. SPE method for the extraction of NE from tissue .....65

Table 4.9. Concentrations of NE determined by HPLC-EC with BND for each tissue and type of rat model as determined by standard addition.....72

**Table 4.10. Concentrations of NE, determined by HPLC-EC with a BND electrode in the different chambers of the rat heart from normotensive, Sham, DOCA-salt and 6-OHDA animals.....76**

## LIST OF FIGURES

### Chapter 1: Introduction

Figure 1.1. Catechol - the base of the catecholamine, and norepinephrine (NE) - a catecholamine neurotransmitter in the sympathetic nervous system.....1

Figure 1.2.  $sp^2$ -carbon microstructure (e.g., glassy carbon) and representative functional groups that terminate the edge-plane sites .....4

Figure 1.3. The  $sp^3$  bonded carbon microstructure of cubic diamond .....5

### Chapter 2: Experimental Methods

Figure 2.1. Diagram of the single compartment, glass electrochemical cell .....9

Figure 2.2. A modular diagram of the commercial RP-HPLC system used in this work.....11

Figure 2.3. Diagram of the thin-layer, cross-flow electrochemical detection cell .....12

Figure 2.4. 6-Hydroxydopamine (6-OHDA), a neurotransmitter analogue, that is a neurotoxin destroying adrenergic nerve terminals in the periphery and dopaminergic nerves in the brain.....16

### Chapter 3: Cyclic Voltammetry of Norepinephrine at Boron-Doped Nanocrystalline and Microcrystalline Thin-Film Electrodes

Figure 3.2. Cyclic voltammetric i-E curves for (A) 1 M KCl (B) 1.0 mM  $Fe(CN)_6^{3/4-}$  and (C) 1.0 mM  $Ru(NH_3)_6^{3/2+}$  (both in 1 M KCl). Detection electrode = BND. Scan rate = 100 mV/s. Electrode geometric area = 0.20 cm<sup>2</sup>. Scans 9 – 10 shown .....22

Figure 3.3. Cyclic voltammetric i-E curves for 50 mM phosphate buffer, pH 2-7 recorded on BMD and BND. Scan rate = 100 mV/s. Electrode geometric area = 0.20 cm<sup>2</sup> .....25

Figure 3.4. Background current at 500 mV vs Ag/AgCl for BND and BMD as a function of the solution pH. Electrolyte = 50 mM phosphate buffer. Scan rate = 100 mV/s. Electrode geometric area = 0.20 cm<sup>2</sup>. Error bars represent the standard deviation of the background current for 3 electrodes of each type (n = 3).26

Figure 3.5. The reversible electrochemical oxidation of NE to noradrenoquinone (NE-quinone).....	27
Figure 3.6. Cyclized NE observed at higher pH (>4). This is the reversible reaction for peaks 3 and 4.....	28
Figure 3.7. Intramolecular cyclization of the protonated NE-quinone .....	29
Figure 3.8. Cyclic voltammetric i-E curves for 25 $\mu$ M NE in 50 mM phosphate buffer at various pH. Detection electrode = BMD. Scan rate =100 mV/s. Electrode geometric area = 0.2 cm <sup>2</sup> . Scans 9-10 shown for pH 2-6, scans 1-3 shown for pH 7 .....	31
Figure 3.9. Cyclic voltammetric i-E curves for 25 $\mu$ M NE in 50 mM phosphate buffer at various pH. Detection electrode = BND. Scan rate =100 mV/s. Electrode geometric area = 0.2 cm <sup>2</sup> . Scans 9-10 shown for pH 2-6, scans 1-3 shown for pH 7 .....	32
Figure 3.10. i-E curves for 25 $\mu$ M NE in 0.1 M phosphate buffer (pH 7.2) recorded as a function of scan rate. Scan rates 100, 300, 500, 700 and 1000 mV/s. Scans 9-10 shown. All i-E curves are background corrected .....	33
Figure 3.11. Dependence of peak oxidation current ( $i_p$ ) on square root of the scan rate ( $v$ ) at BMD and BND in 25 $\mu$ M NE. Electrolyte = 50 mM phosphate buffer, pH 2. BMD $R^2 = 0.99$ ; BND $R^2 = 0.99$ . Electrode area = 0.2 cm <sup>2</sup> , reference electrode = Ag/AgCl. 0.20 cm <sup>2</sup> , $y = 8.70x$ ; 0.13 cm <sup>2</sup> , $y = 5.67x$ ; BND, $y = 5.30x + 0.20$ ; BMD, $y = 5.50x + 0.25$ .....	34
Figure 3.12. A plot of peak anodic current for 25 $\mu$ M NE at BMD and BND as a function of solution pH. Electrolyte = 50 mM phosphate buffer. Electrode area = 0.2 cm <sup>2</sup> , reference electrode = Ag/AgCl. Scan rate = 100 mV/s .....	36
Figure 3.13. A plot of peak potential for 25 $\mu$ M NE at BMD and BND as a function of solution pH. Electrolyte = 50 mM phosphate buffer. Electrode area = 0.2 cm <sup>2</sup> , reference electrode = Ag/AgCl .....	37
Figure 3.14. A plot of $\Delta E_p$ ( $E_p^{ox} - E_p^{red}$ ) for 25 $\mu$ M NE at BMD and BND as a function of solution pH. Electrolyte = 50 mM phosphate buffer, pH 2. Electrode area = 0.2 cm <sup>2</sup> . Reference electrode = Ag/AgCl.....	39
Figure 3.15. Chronocoulogram of 25 $\mu$ M NE at freshly polished GC. Electrolyte = 100 mM phosphate buffer, pH 7.2. Electrode area = 0.2 cm <sup>2</sup> . Reference electrode = Ag/AgCl. A 5-second double-potential step waveform was used where $E_1 = -0.5$ V, $E_2 = 0.8$ V. ....	41

Figure 3.16. Chronocoulograms of 25  $\mu\text{M}$  NE at BND and BMD. Electrolyte = 100 mM phosphate buffer, pH 7.2. Electrode area = 0.2  $\text{cm}^2$ . Reference electrode = Ag/AgCl. A 5-second double-potential step waveform was used where  $E_1 = -0.5 \text{ V}$ ,  $E_2 = 1 \text{ V}$ . .....42

**Chapter 4: Determination of Norepinephrine in Normal, Sham, DOCA-salt and 6-Hydroxydopamine treated Rat Tissue by Reversed-Phase HPLC Separation and Amperometric Detection using a Boron-Doped Nanocrystalline Diamond Thin-Film Electrode**

Figure 4.1. Norepinephrine and epinephrine metabolic pathways.....44

Figure 4.2. The chemical composition of the Supelco Discovery HS-F5 stationary phase.....48

Figure 4.3. Hydrodynamic voltammogram obtained for 10  $\mu\text{M}$  NE at BND. Column = Supelco Discovery HS-F5 (150 mm x 4.6 mm, 5  $\mu\text{m}$ ) equipped with guard column (20 mm x 4.6 mm, 5  $\mu\text{m}$ ), mobile phase = 50 mM ammonium formate buffer (pH 3), flow rate = 1 mL/min, injection volume = 20  $\mu\text{L}$  .....53

Figure 4.4. Response curve for NE at BND.  $R^2 = 0.999$ . Mobile phase = 50 mM ammonium formate buffer (pH 3), detection potential = 950 mV vs. Ag/AgCl, flow rate = 1 mL/min .....54

Figure 4.5. Chromatogram for several catecholamines (NE, EP, DA) and metabolites (DOPEG, NM, VMA, MN). All solute concentrations were 10  $\mu\text{M}$ . Detection electrode = BND. The mobile phase was 50 mM ammonium formate buffer (pH 3). Flow rate = 1 mL/min. Injection volume = 20  $\mu\text{L}$ . Detection potential = 950 mV vs. Ag/AgCl.....55

Figure 4.6 – A chromatogram for a direct injection of the filtered supernatant from a left ventricle sample (upper trace) and a 1  $\mu\text{M}$  NE standard solution (lower trace). The detection electrode was BND.  $E_{\text{det}} = 950 \text{ mV}$  (vs. Ag/AgCl). Flow rate = 1 mL/min. Injection volume = 20  $\mu\text{L}$ . Mobile phase = 50 mM ammonium formate buffer (pH 3) .....62

Figure 4.7. The molecular structure of the Oasis MCX polymeric sorbent and interaction sites.....64

Figure 4.8. Chromatogram of liver extract from a DOCA-salt rat. The chromatogram shows a late eluting peak which has caused interference in a subsequent analysis. A small peak, presumably NE can be seen on the edge of the larger peak following. Detection electrode = BND.  $E_{\text{det}} = 950 \text{ mV}$  (vs.

Ag/AgCl). Flow rate = 1 mL/min. Injection volume = 20  $\mu$ L. Mobile phase = 50 mM ammonium formate buffer (pH3).....70

Figure 4.9 – Chromatograms of (A) spleen extract from a DOCA-salt treated animal and (B) left atrium extract from a normotensive animal. Detection electrode = BND.  $E_{det}$  = 950 mV (vs. Ag/AgCl). Flow rate = 1 mL/min. Injection volume = 20  $\mu$ L. Mobile phase = 50 mM ammonium formate buffer (pH3).....71

Figure 4.10. Concentration of NE found in the tissues from different normotensive, Sham, and DOCA-salt rats. The concentrations were determined by HPLC-EC with BND. LK = left kidney, SI = small intestine.....72

Figure 4.11. Chromatograms of a right ventricle extract from a DOCA-salt rat before (A) and after 0.5  $\mu$ L spikes of a 100  $\mu$ M NE stock solution (B-F). stacked accordingly. The detection electrode was BND.  $E_{det}$  = 950 mV (vs. Ag/AgCl). Flow rate = 1 mL/min. Injection volume = 20  $\mu$ L. Mobile phase = 50 mM ammonium formate buffer (pH3).....74

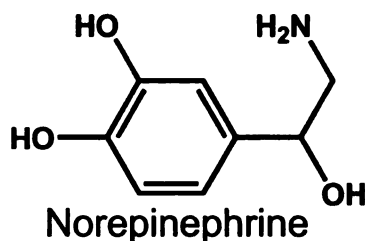
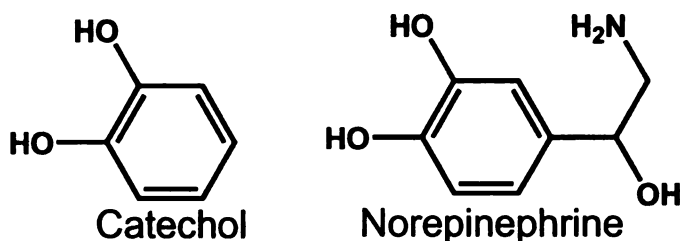
Figure 4.12 – Concentrations of endogenous NE found in different chambers of the rat heart as determined by HPLC-EC with BND electrode. LA – left atrium; RA – right atrium; LV – left ventricle; RV – right ventricle; VSW – ventricular septal wall.....75

Figure 4.13. BND response stability for NE over an 83 day period (hundreds of injections). Injections of 1  $\mu$ M NE standard were made using a single electrode with no maintenance.  $E_{det}$  = 950 mV (vs. Ag/AgCl). Flow rate = 1 mL/min. Injection volume = 20  $\mu$ L. Mobile phase = 50 mM ammonium formate buffer (pH3). Each point represents the average of 3 separate injections .....79

# Chapter 1

## Introduction

Catecholamines are a class of neurotransmitters that have very diverse functions throughout the central and peripheral nervous system. They have a common structure consisting of a six-membered aromatic ring with two hydroxyl groups at the 1 and 2 positions. This base is a catechol and its molecular structure is shown in Figure 1.1. These molecules and their metabolites play important roles in a multitude of physiological processes, and are related to the etiology of neurological, psychiatric, endocrine and cardiovascular diseases.<sup>[1, 2]</sup> The involvement of these neurochemicals in eating disorders, Parkinson's disease and hypertension make them targets for research. Their importance in hypertension is the motivation for our work.<sup>[3, 4]</sup>



**Figure 1.1.** Catechol - the base structure of the catecholamine, and norepinephrine (NE) - a catecholamine neurotransmitter in the sympathetic nervous system.

Hypertension is broadly defined as a chronic elevation of blood pressure (systolic > 150 mm Hg). Often there are no obvious symptoms with this disease; hence it is termed the “silent killer”. Prolonged hypertension increases one’s risk of coronary heart disease (which leads to heart attack), stroke, and kidney failure. Data from the National Health and Nutrition Examination Survey collected from 1999-2002 shows that the number of Americans age 20 and older with hypertension is over 65 million. This represents a rise of approximately 30% over the last decade.<sup>[5]</sup> These statistics illustrate the need for basic research into the causes of hypertension. It is imperative that the causes and physiological mechanisms behind hypertension be understood so that therapeutic treatments can be developed.

It has been established that essential hypertension (i.e., hypertension with no known cause) is initiated and sustained by overactivity of the sympathetic nervous system (SNS).<sup>[4]</sup> Within the mammalian SNS, norepinephrine (NE) is the principle neurotransmitter. Although the causal mechanisms are unclear, it is speculated that increases in sympathetic nerve firing rates, NE efflux per firing event, smooth muscle cell innervation, and inhibition of the norepinephrine reuptake process may be of significance. Evidence of overactivity of the SNS is the elevated circulating NE levels found in hypertensive humans and rats (i.e., greater spillover).<sup>[4]</sup> The structure of NE is shown in Figure 1.1.

In order to better understand how sympathetic neural control mechanisms are altered in hypertension, steps must be taken to isolate and detect NE. The purpose of the research reported on herein was development of an analytical

method useful for determining NE content in the organs of healthy and diseased rats. The method involved, first, sample pretreatment and clean-up involving extraction of NE from tissue homogenate. The next step was a reversed-phase high-performance liquid chromatography (RP-HPLC) separation. RP-HPLC is a well-established technique for this type of analysis with published papers covering 35 years. A key feature of the analysis was amperometric detection using a boron-doped diamond thin-film electrode. Catechols and catecholamines are electrochemically-active and, therefore, are ideally suited for electrochemical detection. NE is oxidized to the corresponding quinone via a  $2 H^+ / 2 e^-$  reaction.<sup>[6]</sup>

One goal of the project was to determine how effective diamond electrodes are for the detection of catecholamines in biological fluids. Diamond is a relatively new electrode that has some outstanding properties. There has been work published on using diamond to monitor environmental contaminants<sup>[7, 8]</sup>, but very little on its use in bioanalysis. Related work has shown that boron-doped diamond can be used for the amperometric detection of neurogenic amines and for *in vivo* monitoring of neuronal release of norepinephrine. So far there has been very little reported on the use of the boron-doped diamond planar electrodes for bioanalysis.<sup>[4, 9-13]</sup>

Diamond possesses properties attractive for bioanalysis. Commonly used carbon electrodes are composed of an  $sp^2$  bonded microstructure that contains many electroactive, ionizable carbon-oxygen functionalities, as depicted in Figure 1.2.<sup>[14]</sup> These surface functional groups can complicate electrochemical

measurements by causing increased and pH-dependent background current. Such polar electrodes are also susceptible to fouling by strong molecular adsorption and need frequent pretreatment for activation. This leads to considerable response variability.<sup>[6]</sup>

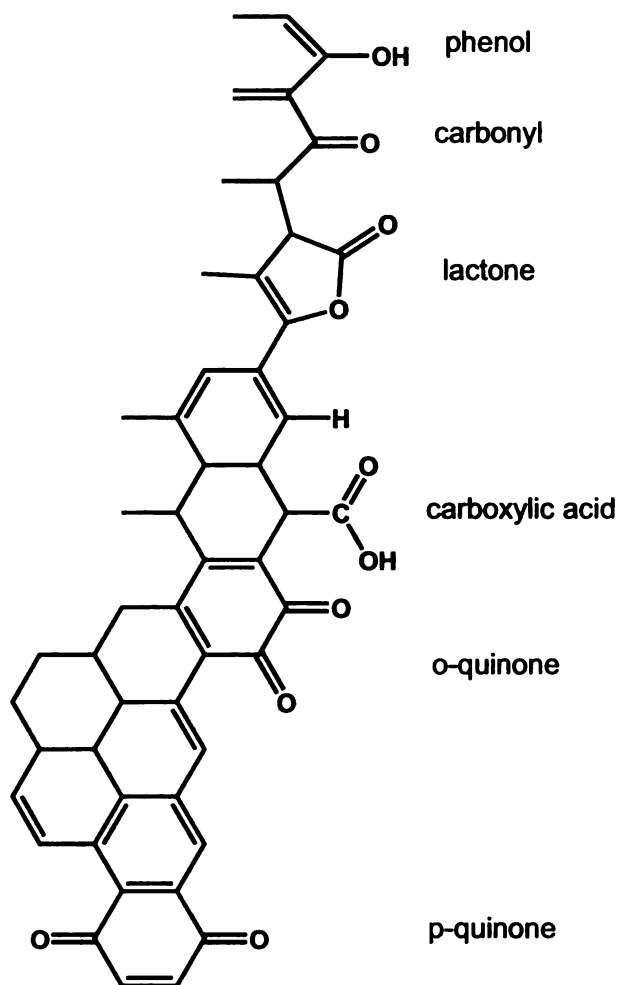


**Figure 1.2.** sp<sup>2</sup>-carbon microstructure (e.g., glassy carbon) and representative functional groups that terminate the edge-plane sites.<sup>[6]</sup>

Diamond, on the other hand, is composed of a sp<sup>3</sup>-bonded microstructure, with a hydrogen-terminated surface, as illustrated in Figure 1.3. Diamond is the stable form of carbon at high pressure and temperature.<sup>[15]</sup> The surface carbon

atoms are stabilized by strong covalent bonds with hydrogen for films deposited from hydrogen-rich source gas mixtures. Pure diamond is an electrical insulator; however, it can be made semimetallic when doped with boron. A typical resistivity for a highly doped film is  $<0.01 \Omega - \text{cm}$ , making it sufficiently conducting to be used as an electrochemical electrode. The electrical conductivity is controlled primarily by the boron-doping level, but also by the grain boundary density and the nondiamond  $\text{sp}^2$  carbon impurity that might be present.<sup>[6]</sup>

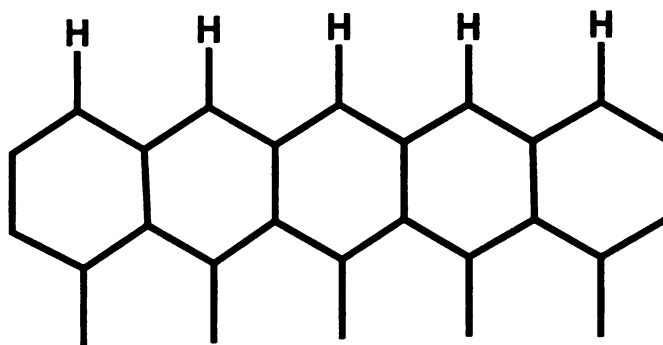


**Figure 1.3.** The  $\text{sp}^3$  bonded carbon microstructure of cubic diamond.

Boron-doped diamond (BDD) possesses outstanding electrochemical properties: a low and stable background current over a wide potential range, good responsiveness for many redox analytes without pretreatment, superb microstructural stability and resistance to fouling because of weak adsorption of polar species on the hydrogen terminated surface.<sup>[6, 9, 12, 16]</sup> These properties make BDD a logical choice when making measurements on complex samples that may cause rapid fouling of  $\text{sp}^2$  carbon electrodes.

The specific aims of this research were:

1. To study by cyclic voltammetry the electrochemical behavior of NE at microcrystalline and nanocrystalline diamond thin-film electrodes as a function of the solution pH in order to learn more about the reaction mechanism.

2. To determine how effective the diamond thin-film electrodes are for the analysis of catechols and catecholamines in standard solutions and biological samples. The performance of diamond was assessed in terms of several detection figures of merit (linear dynamic range, sensitivity, limit of detection, response precision, and response stability) and was compared with glassy carbon.

3. To develop an off-line solid phase extraction procedure for separating NE from tissue homogenates prior to separation and detection by RP-HPLC-EC. The method was optimized and applied for the analysis of the spleen, large intestine, kidney and heart of healthy and diseased test animals.

It is important to evaluate the full breadth of the disease, and this involves tracking the changes that occur in the body ranging from anywhere from nerve firing-rates and innervation of muscle cells to that of the levels of neurotransmitters contained in tissue and plasma. The method described in this work was an attempt to create a cost-effective, low-maintenance, simplified approach for tissue analysis capable of high-throughput sample analysis.

## Chapter 2

### Experimental Methods

#### Instrumentation

##### 2.1 Boron-Doped Diamond Thin Film Growth

The diamond thin film was deposited on a p-type Si(100) substrate ( $<10^{-3}$   $\Omega$ -cm, Virginia Semiconductor Inc.) using a commercial microwave-assisted chemical vapor deposition (CVD) system (1.5 kW, 2.54GHz, ASTeX, Inc., Woburn, MA). The substrate surface was mechanically scratched by hand for several minutes on a felt polishing pad with  $\leq 2\mu\text{m}$  diameter diamond powder (Diamond Innovations, OH). The scratched substrate was then rinsed thoroughly with ultrapure water, isopropyl alcohol (IPA), and acetone followed by 3 min of sonication each in acetone, IPA, and finally, ultrapure water to ensure complete removal of all polishing debris. The cleaned substrate was then placed in the CVD reactor.

The microcrystalline diamond film (BMD) was grown using a 0.5% methane ( $\text{CH}_4$ )/hydrogen ( $\text{H}_2$ ) source gas mixture at a total flow of 200 sccm, a microwave power of 1000 W, a growth pressure of 45 torr, a substrate temperature of  $\approx 800$

°C (measured with an optical pyrometer), and a growth time of 10 h. Ultrahigh purity (99.999%) CH<sub>4</sub> and H<sub>2</sub> were used as the source gases. Diborane (B<sub>2</sub>H<sub>6</sub>), diluted in hydrogen (0.1%), was added for boron doping at a concentration of 1 ppm. The plasma was ignited with all gases flowing to initiate the deposition. After growth, the CH<sub>4</sub> and B<sub>2</sub>H<sub>6</sub> flows were stopped and the film remained exposed to the H<sub>2</sub> plasma for an additional 10 min. After this period, the microwave power and system pressure were gradually reduced down to 400 W and 10 mtorr over a 15 min period to cool the sample in the presence of atomic hydrogen. This ensured maximal hydrogen surface termination and removed any non-diamond sp<sup>2</sup> carbon impurity. The film thickness was 4 - 6 μm and the in-plane resistivity was 0.05 Ω-cm, or less.

The nanocrystalline diamond film (BND) was synthesized using ultrahigh purity CH<sub>4</sub>, Ar, and H<sub>2</sub> (99.999%) at flow rates of 1, 94, and 5 sccm, respectively. B<sub>2</sub>H<sub>6</sub>, diluted in hydrogen (0.1%), was added for doping at a concentration of 1 ppm. The microwave power and deposition pressure were maintained at 800 W and 140 torr, respectively, and the substrate temperature was ≈ 700 °C during a 2-h deposition. The plasma was ignited with all gases flowing to initiate the deposition. At the end of the deposition period, the CH<sub>4</sub> and B<sub>2</sub>H<sub>6</sub> flows were stopped while the Ar and H<sub>2</sub> flows continued. The film then remained exposed to the H<sub>2</sub>/Ar plasma for 10 min. The substrate was then cooled in the presence of atomic hydrogen to an estimated temperature of less than 400 °C by slowly reducing the power and pressure over a 10 min period. The resulting diamond film was 4 - 7 μm thick with a resistivity of 0.3 Ω-cm, or less.

## 2.2 Cyclic Voltammetry (CV)

Electrochemical characterization of the BMD and BND films was performed by cyclic voltammetry using several common redox analytes. CV measurements were performed in freshly prepared solutions of 1.0 mM potassium ferrocyanide ( $\text{K}_4\text{Fe}(\text{CN})_6$ , Aldrich) and 1.0 mM hexamine ruthenium(III) chloride ( $\text{Ru}(\text{NH}_3)_6\text{Cl}$ , Aldrich). The supporting electrolyte was 1.0 M potassium chloride (KCl, Fisher). CV was performed with a CHI832A digital potentiostat (CH Instruments) using a single compartment, three-electrode glass cell. The cell design is shown in the figure below.

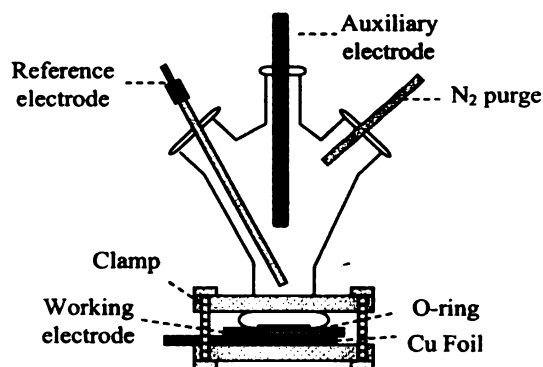


**Figure 2.1.** Diagram of the single compartment, glass electrochemical cell.

The planar working electrode was pressed against a smooth glass joint at the bottom of the cell. A Viton™ O-ring was used to define the geometric area

exposed to the solution, which was 0.2 cm<sup>2</sup>. A large-area carbon rod served as the auxiliary electrode and was positioned normal to the working electrode. An Ag/AgCl electrode, housed in a cracked-glass capillary filled with a saturated KCl solution was used as the reference. All potentials reported herein are with respect to this reference.

### 2.3 Reversed-Phase High Performance Liquid Chromatography

A commercial Shimadzu HPLC system consisting of a control unit (SCL-10Avp), solvent delivery module (LC-10ADvp), degasser (DGU-14A), and an autoinjector (SIL-10ADvp) was used for all HPLC studies presented herein. A flow rate of 1.0 mL/min and an injection volume of 20 µL was used for all separations unless mentioned otherwise. Figure 2.2 shows a modular diagram of the HPLC-EC system used in this work. Three different columns were evaluated: Adsorbosphere HS C<sub>18</sub> (5 µm, 4.6 mm I.D. x 150 mm) from Alltech, XTerra RP<sub>18</sub> column (5 µm, 4.6 mm I.D. x 150 mm) from Waters, and Discovery HS F5 column (5 µm, 4.6 mm I.D. x 150 mm) from Supelco.

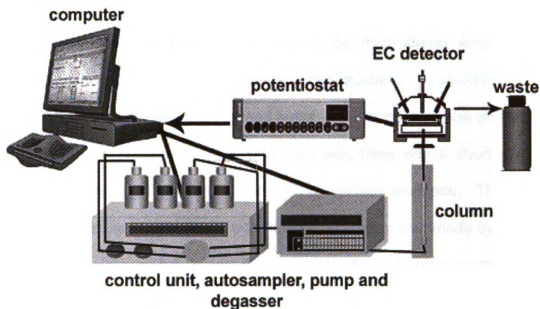


**Figure 2.2.** A modular diagram of the commercial RP-HPLC system used in this work.

The Discovery column was found to perform the best in terms of capacity factor, selectivity factor and reproducibility, and was therefore used for this work. All separations were performed with a precolumn (guard) to protect the analytical column from fouling. The mobile phase was 50 mM ammonium formate buffer adjusted to pH 3 with concentrated formic acid. Detection was accomplished amperometrically using a thin-layer flow cell, described below, which housed the working, reference and auxiliary electrodes.

#### 2.4 Thin-Layer Flow-Cell

The entire set-up was electrically grounded and the flow cell was housed in a Faraday cage to reduce the interference from strong environmental electromagnetic radiation. The flow cell was constructed with two pieces of Kel-F. The top piece contained the inlet and outlet ports for the fluid flow and a place for the reference electrode. The outlet port was fitted with a short piece of stainless steel tubing that also served as the auxiliary electrode. The bottom piece supported the working electrode. Electrical contact was made by pressing a piece of clean copper foil against the back side of the planar diamond working electrode.

A rubber gasket separated the surface of the working electrode from the top piece of the cell. A rectangular groove (0.80 cm x 0.15 cm x 0.10 cm) was cut into the gasket which defined the flow channel. Assuming a 25% compression of the gasket, when the top and bottom pieces of the cell were clamped together, the cell volume was estimated to be ~9  $\mu\text{L}$ .

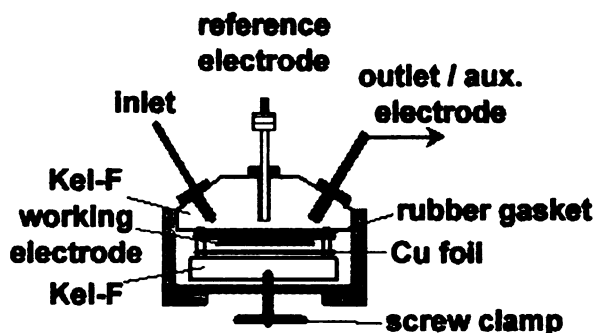


**Figure 2.3.** Diagram of the thin-layer, cross-flow electrochemical detection cell.<sup>[17]</sup>

The potential applied to the working electrode and the resultant current were measured using an Omni-90 analog potentiostat (Cypress Systems Inc.). The potential was applied with respect to a commercial 66-EE009 "no-leak" Ag/AgCl reference electrode (Cypress Systems Inc.). Data were acquired by an internal analog board located in the system controller unit and analyzed by computer with Shimadzu Class VP software (v. 7.3sp1).

## **Animals**

### **2.5 Heart Tissue Preparation**

Six 8-week old adult male Sprague-Dawley rats, (from Charles River, Portage, MI) weighing 250-275 g were used in these studies. All animal procedures were in accordance with the guidelines set forth by the Institutional Animal Care & Use Committee (IACUC) of Michigan State University. The animals were randomly divided into control (untreated), Sham, DOCA-salt and denervated (6-OHDA treated) groups, and housed two per cage in the same treatment group in a temperature and humidity-controlled room with a 12-h light/dark cycle. The animals were provided with standard pellet rat chow and water *ad libitum*.

## 2.6 Preparation of DOCA-salt Hypertensive and Sham Rat Models

The rats were anesthetized with sodium pentobarbital (50 mg/kg, intra-peritoneal). The skin over the left flank (lateral abdominal wall) was shaved and cleaned with an iodine-based antiseptic. A 1.5-cm vertical incision was then made through the skin and the underlying muscle just caudal to the rib cage. The left kidney was exteriorized and removed after ligation of the renal artery, vein and ureter with 4-0 silk sutures. The muscle and skin layers were closed separately with 4-0 silk and 4-0 monofilament nylon sutures, respectively. A 3×1.5-cm rectangular area between the shoulder blades was then shaved and disinfected prior to subcutaneous DOCA implantation in a 1-cm incision. The skin was closed with 4-0 nylon sutures. DOCA implants (600 mg/kg) were prepared by mixing deoxycorticosterone acetate in silicone rubber, resulting in a dosage of 200 mg/kg.

Sham-operated rats underwent left kidney removal only. Surgery was performed on a heated pad and rats recovered in a heated box. Antibiotics (enrofloxacin, 5 mg/kg, s.c.) and analgesic (butorphanol tartrate, 2 mg/kg, s.c.) were administered immediately after surgery. After recovery, the rats were housed under standard conditions for 4 weeks. DOCA-implanted rats received standard pelleted rat chow and salt water (1% NaCl+0.2% KCl) *ad libitum*, while sham rats received standard pelleted rat chow and tap water *ad libitum*. Systolic

blood pressure was measured using the tail-cuff method 4 weeks after surgery. Rats with a sustained systolic blood pressure equal to or higher than 150 mm Hg were considered hypertensive.

## 2.7 Treatment with 6-OHDA

6-Hydroxydopamine (6-OHDA), whose molecular structure is shown in Figure 2.3, is a neurotoxin that is routinely administered to sympathectomize rats. 6-OHDA binds to NE-transporter protein, whereby it is then taken into the nerve terminal. Once inside the nerve terminal it forms a reactive quinone that can then interact with thiol groups on membrane proteins and form peroxides with membrane lipids. This interaction causes decay of the nerve terminal. 6-OHDA selectively destroys adrenergic nerve-endings, which markedly depletes NE from the peripheral organs by reversibly eliminating NE uptake and storage.<sup>[18, 19]</sup>

6-Hydroxydopamine (6-OHDA) was prepared fresh in a mixture of 0.9 % (154 mM) sodium chloride and 0.5 % (28.4 mM) ascorbic acid before application and was stored in the dark to prevent degradation. Animals were dosed according to body weight (250 mg/kg) with a subcutaneous injection of the neurotoxin 6-OHDA. The 6-OHDA was administered using a 25 gauge needle to the loose skin between the shoulder blades using 3 injections over a one week period on days 1, 3 and 5. On day 7, two days after the final dose, the animals were sacrificed. Age and sex matched control animals were untreated.

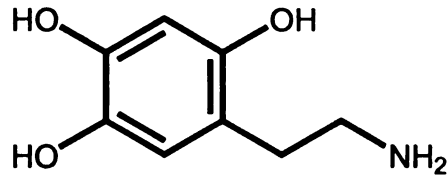


**Figure 2.4.** 6-Hydroxydopamine (6-OHDA), a neurotransmitter analogue, that is a neurotoxin destroying adrenergic nerve terminals in the periphery and dopaminergic nerves in the brain.

## 2.8 Tissue collection

Rats were anesthetized with a lethal dose of sodium pentobarbital (65 mg/kg, intra-peritoneal) followed by thoracotomy. Hearts were removed while beating and immediately placed into chilled (4 °C) phosphate buffered saline, containing 137 mM sodium chloride, 2.7 mM potassium chloride, 4.3 mM sodium phosphate dibasic and 1.4 mM potassium phosphate monobasic, for separation of chambers. While in buffer, the chambers were quickly separated in the following order: right atrium, left atrium, right ventricle outer wall, ventricular septal wall, and left ventricle outer wall. Dissected chambers were frozen immediately by contact with dry ice and stored at -80 °C until further processing.

## 2.9 Tissue sample homogenization

A frozen piece of tissue was first weighed and then homogenized using a variable speed Omni TH-115 homogenizer with 5 mm saw tooth generator probe (Omni International Inc., Warrenton, VA) in ice-cold 0.1 M perchloric acid, 2 mL / 0.5 g (left ventricle, right ventricle, ventricular septum) and 5 mL / 0.5 g (right and left atrium), for ~ 3 min at 30,000 rpm. The homogenate was then centrifuged at 13,500 rpm for 15 min at 4°C. The supernatant was then processed by solid phase extraction (SPE) prior to analysis by HPLC.

## 2.10 SPE Procedure

A modified version of a Waters Oasis MCX methodology for the extraction of NE was used for additional sample clean-up and analyte (NE) preconcentration. Oasis MCX cartridges (1 mL, Milford, MA) filled with 30 mg of sorbent having a 30 µm particle size and an 80 Å pore size were used. The solid phase extraction was performed using a 12-port vacuum manifold from Alltech Associates, Inc. (Deerfield, IL). Sample supernatant (0.5 - 1.0 mL) was loaded onto a conditioned SPE cartridge at a flow rate < 0.5 mL/min. The elution time was approximately 25 min. The column pre-conditioning involved sequential passage of 1 mL of methanol and 2 mL of ultrapure water through sorbent material.

The cartridge washing was performed by two 1-mL washings of 0.1 M hydrochloric acid aliquots followed by two 1-mL washings of methanol. The loaded column was then dried under vacuum for 6 min prior to analyte elution.

Elution was accomplished by passing of 0.5 – 1 mL (same volume as used for sample loading) of borate buffer, 250 mM boric acid/KOH, pH 8.8, through the SPE sorbent material (< 0.5 mL/min). The eluate was then directly injected into the HPLC system. Recoveries were defined by the percent concentration extracted and eluted determined by the analyte peak height obtained through analysis by our HPLC-EC system. The recoveries were calculated by extracting 1  $\mu$ M solutions of NE and E in perchloric acid by SPE. The preconcentration factor in this work was 1.

## 2.11 Materials and Chemicals

(-)-Norepinephrine (NE), dopamine hydrochloride (DA), (R)-(-)-epinephrine (E), DL-normetanephrine hydrochloride (NM), 5-hydroxytryptamine (serotonin, 5-HT), 4-hydroxy-3-methoxybenzylamine (HMBA), 1-heptanesulfonic acid (HSA), DL-4-hydroxy-3-methoxymandelic acid (VMA), DL-metanephrine hydrochloride (MN), and 6-hydroxydopamine hydrobromide (6-OHDA) were purchased from Sigma-Aldrich Co. (St. Louis, MO). The chemicals were high quality (>98 % pure) and used without additional purification.

The chemicals used for the preparation of the mobile phase buffer were ammonium formate (ultra-high purity, 99%, Fluka Co., USA) and formic acid (high purity, Riedel – de Haen, Germany). Sodium hydroxide and sodium metabisulfite and disodium hydrogen phosphate was obtained from Spectrum

Quality Products, (Gardena, CA), and potassium hydroxide was obtained through Columbus Chemical Industries (Columbus, WI). Sodium dihydrogen phosphate was obtained from J. T. Baker (Phillipsburg, NJ). Tissue homogenization was performed in 0.1 M perchloric acid (ultrahigh purity, 99.999%, Sigma-Aldrich Co.).

Stock solutions of NE, E, D, 5-HT, NM and HMBA (10 mM) were prepared in a stabilizing solution containing 100 mg sodium metabisulfite, 800 mg sodium chloride (Jade Scientific, Canton, MI) and 500  $\mu$ L 37% hydrochloric acid (ultrahigh purity, 99.999%, Sigma-Aldrich Co.) dissolved in 100 mL of ultrapure water.<sup>[2, 20]</sup> Methanol used in SPE procedure was HPLC grade, obtained from Sigma-Aldrich Co. (St. Louis, MO). Ultrapure 18 M $\Omega$  water (Barnstead E-Pure System, Barnstead International, Dubuque, IA) was used for all solution preparation.

## **Chapter 3**

# **Cyclic Voltammetry of Norepinephrine at Boron-Doped Microcrystalline and Nanocrystalline Diamond Thin-Film Electrodes**

### **3.1 Introduction**

In a voltammetric measurement, a potential is applied to the working electrode with respect to the fixed potential of a reference electrode. This potential serves as the driving force for a redox reaction and the resultant current that flows is measured. The working electrode acts as a sink or source for electrons. The current measured can be used to determine the redox analyte concentration in solution.<sup>[21]</sup>

Electrochemical detection of catecholamines is a sensitive method with good precision.<sup>[22-25]</sup> A limitation of EC detection is the need for electrode pretreatment, at least for most electrodes. Classically used electrodes, such as carbon paste or glassy carbon, are subject to fouling due to the adsorption of airborne contaminants, reaction intermediates and products during analysis.<sup>[16, 26]</sup>

The experiments reported on herein were carried out using boron-doped diamond (BDD). Currently, two types of BDD are synthesized in-house; boron-doped nanocrystalline (BND) and microcrystalline (BMD) thin-film. BDD electrodes exhibit a wide working potential window, resistance to response attenuation by fouling, microstructural and morphological stability at high potentials and long-term response stability. Also, pretreatment is not required to ready the electrode for use.<sup>[9, 27]</sup> Both BMD and BND possess a hydrogen terminated sp<sup>3</sup>-bonded carbon microstructure, which accounts for many of the above listed qualities. BMD possesses a well-faceted polycrystalline morphology with crystallites of  $\geq 2 \mu\text{m}$ , while the BND has a smoother texture with smaller crystallites, 50 nm or less in size.<sup>[9]</sup>

BND was used in most of this work based on direct comparison of measurements which showed that the electrode possessed better response precision and greater sensitivity for NE, DA and catechol.<sup>[6]</sup> A supplemental discussion and comparison of GC, BND and BMD electrodes for catecholamine analysis and determination can be found elsewhere.<sup>[6]</sup>

### 3.2 Electrochemical Characterization of Diamond Electrodes

BMD and BND electrodes were initially characterized by cyclic voltammetry (CV) using several redox couples. The geometric area of the electrode exposed to the solution was 0.20 cm<sup>2</sup>. While in the electrochemical cell (Fig. 2.1), the electrode was soaked in distilled isopropyl alcohol for 10 min

prior to use in order to clean the surface.<sup>[28]</sup> 1.0 mM solutions of potassium ferrocyanide ( $\text{Fe}(\text{CN})_6^{3/4-}$ ) and hexamine ruthenium(III) chloride ( $\text{Ru}(\text{NH}_3)_6^{3/2+}$ ), were prepared fresh daily in 1.0 M potassium chloride (KCl). Figure 3.2 shows typical i-E curves for a BND electrode exposed to (A) KCl, (B)  $\text{K}_4\text{Fe}(\text{CN})_6$  and (C)  $\text{Ru}(\text{NH}_3)_6\text{Cl}_3$ .

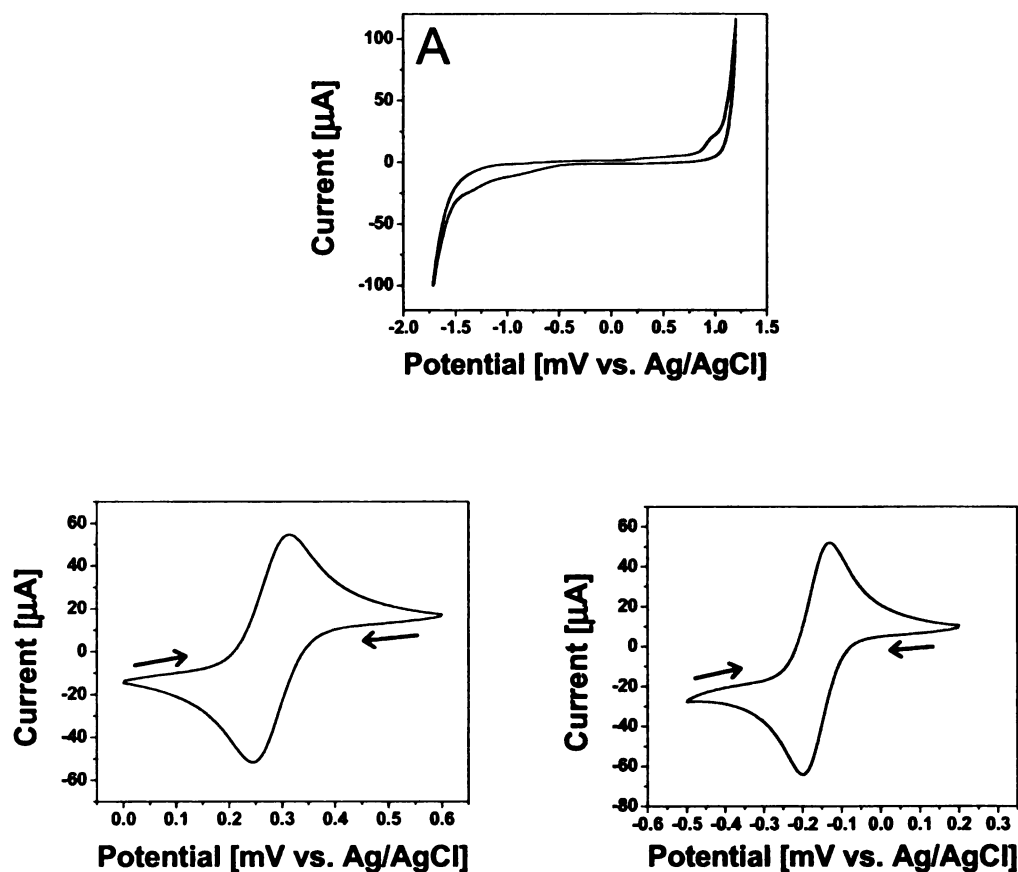


**Figure 3.2.** Cyclic voltammetric i-E curves for (A) 1 M KCl (B) 1.0 mM  $\text{Fe}(\text{CN})_6^{3/4-}$  and (C) 1.0 mM  $\text{Ru}(\text{NH}_3)_6^{3/2+}$  (both in 1 M KCl). Detection electrode = BND. Scan rate = 100 mV/s. Electrode geometric area = 0.20 cm<sup>2</sup>. Scans 9 – 10 shown.

The background voltammogram is featureless over a wide potential range between 1.0 and -1.5 V. The background current at these potentials is low and stable with cycling. Presumably, the anodic current flowing at 1.5 V is due to chlorine evolution and the cathodic current at -1.5 V is due to hydrogen evolution. There is a small anodic peak at about 0.950 V, just prior to onset of chlorine evolution. The origin of this peak is unknown but has been attributed by others to the oxidation of sp<sup>2</sup> carbon impurity in the grain boundary.<sup>[29]</sup> The i-E curves for both redox systems are well-resolved and symmetric with two well-defined peaks. The  $i_p^{ox}/i_p^{red}$  ratio is recorded below in Table 3.2. The data for both the BMD and BND are near unity for both redox systems, which is indicative of a reversible system.<sup>[30]</sup> The peak potential separation,  $\Delta E_p = E_p^a - E_p^c$ , is near Nernstian (59/n mV) with a value of 69 mV. The  $\Delta E_p$  increases with increasing scan rate consistent with quasi-reversible electrode-reaction kinetics. The forward peak currents are 57 and 63  $\mu\text{A}$  for  $\text{Fe}(\text{CN}_6)^{-3/-4}$  and  $\text{Ru}(\text{NH}_3)_6^{+2/+3}$ , respectively, and are in good agreement with the theoretically predicted peak currents of 52 and 46  $\mu\text{A}$  obtained using the following equation:

$$i_p = 2.69 \times 10^5 n^{3/2} A D^{1/2} C v^{1/2}$$

The equation parameters are defined as  $i_p$  = peak current (A),  $n$  = stoichiometric number of electrons in the reaction,  $A$  = geometric electrode area ( $\text{cm}^2$ ),  $D$  = diffusion coefficient ( $\text{cm}^2/\text{s}$ )<sup>[16]</sup>,  $C$  = concentration ( $\text{mol}/\text{cm}^3$ ) and  $v$  = scan rate (V/s). The narrow  $\Delta E_p$  value for both redox couples is indicative of rapid electron-transfer kinetics.<sup>[9]</sup>

**Table 3.1.** Comparison of experimentally observed and published values of  $\Delta E_p$  for  $\text{Fe}(\text{CN})_6^{-3/4}$  and  $\text{Ru}(\text{NH}_3)_6^{+3/+2}$ . Experimental values shown are the mean for 3 electrodes of each type along with the relative standard deviation.

	$\text{Fe}(\text{CN})_6^{-3/4} \Delta E_p$ (mV)	$\text{Ru}(\text{NH}_3)_6^{+3/+2} \Delta E_p$ (mV)
<b>BMD Experimental</b>	70 ± 2.5 %	66 ± 0.8 %
<b>BND Experimental</b>	68 ± 3.4 %	69 ± 2.2 %
<b>BMD Literature</b>	65-75 [9, 16]	65-76 [9, 10, 16, 31]
<b>BND Literature</b>	65-75 [9, 16]	59 [9, 11, 16]

**Table 3.2.** Experimental data recorded at BMD and BND for the  $\text{Fe}(\text{CN})_6^{-3/4}$  and  $\text{Ru}(\text{NH}_3)_6^{+3/+2}$  systems.

	<b>BMD</b>	<b>BND</b>
$i_p^{\text{ox}} \text{Fe}(\text{CN})_6^{-3/4}$	58 ± 0.9 % $\mu\text{A}$	58 ± 0.4 % $\mu\text{A}$
$i_p^{\text{ox}} \text{Ru}(\text{NH}_3)_6^{+3/+2}$	63 ± 0.4 % $\mu\text{A}$	63 ± 1.7 % $\mu\text{A}$
$i_p^{\text{ox}}/i_p^{\text{red}} \text{Fe}(\text{CN})_6^{-3/4}$	0.98 ± 0.01%	0.98 ± 0.2%
$i_p^{\text{ox}}/i_p^{\text{red}} \text{Ru}(\text{NH}_3)_6^{+3/+2}$	0.97 ± 0.3%	0.97 ± 0.5%
$E_{p/2} \text{Fe}(\text{CN})_6^{-3/4}$	258 ± 0.6% mV	256 ± 0.2% mV
$E_{p/2} \text{Ru}(\text{NH}_3)_6^{+3/+2}$	187 ± 0.6% mV	187 ± 0.6% mV

### 3.3 Cyclic Voltammetric Behavior of Norepinephrine

Cyclic voltammetry was used to evaluate the behavior of NE at the BMD and BND electrodes over a pH range from 2 to 7. 50 mM phosphate buffer was prepared at pH of 2, 3, 4, 5, 6 and 7. A background CV was first recorded for each electrode in the buffer of each pH after bubbling with nitrogen gas for 10 min to deoxygenate the solution. Following this, CVs were recorded for 25  $\mu\text{M}$  NE as a function of solution pH. Background voltammograms were recorded at pH 2 through 7 and are presented in Figure 3.3.

The background current results from the movement of ions and solvent dipoles which change the electric double-layer, electrochemical reactions on the electrode surface, and the electrolysis of any solution impurities.<sup>[16]</sup> In the case of diamond, the background is almost exclusively due to double-layer charging. The background i-E curves are featureless at each pH studied for BMD except for the expected shifts in the potential limits. The BND background current at pH 2 is the largest with small peaks observed at ~0.7 and ~0.3 V that are attributed to redox processes at the  $sp^2$  carbon in the grain boundary. The surface termination also changes from hydrogen to oxygen during cycling in acidic media.<sup>[27]</sup>

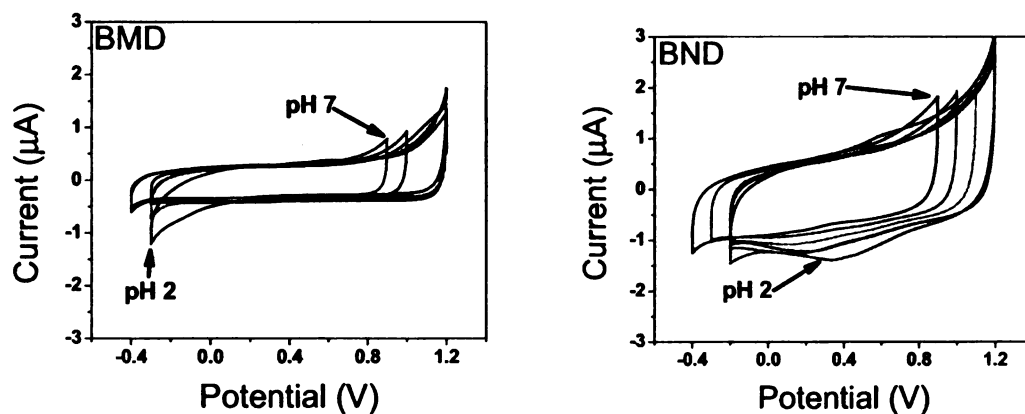


**Figure 3.3.** Cyclic voltammetric i-E curves for 50 mM phosphate buffer, pH 2-7 recorded on BMD and BND. Scan rate = 100 mV/s. Electrode geometric area = 0.20 cm<sup>2</sup>.

The magnitude of the non-faradaic anodic current was recorded in the supporting electrolyte at 500 mV (vs. Ag/AgCl) at each pH. The plots in Figure 3.4 reveal how the background current varied as a function of the pH for both

BND and BMD electrodes. It can be seen that the background current for BND is ~300 nA higher than that for BMD. The reason for this is presumably the increased fraction of exposed grain boundary.<sup>[11]</sup> The background current, per geometric area, for BND is typically a factor of 1-2 larger than the current for BMD. The  $\pi$ -bonded carbon at the grain boundary is a source of charge carriers, which can increase the capacitive component of the background signal.<sup>[11]</sup> The error bars represent the variance of background current for 3 electrodes. The BND electrodes have a larger variation from electrode to electrode whereas the BMD electrodes demonstrated background current with less inter-electrode fluctuation.

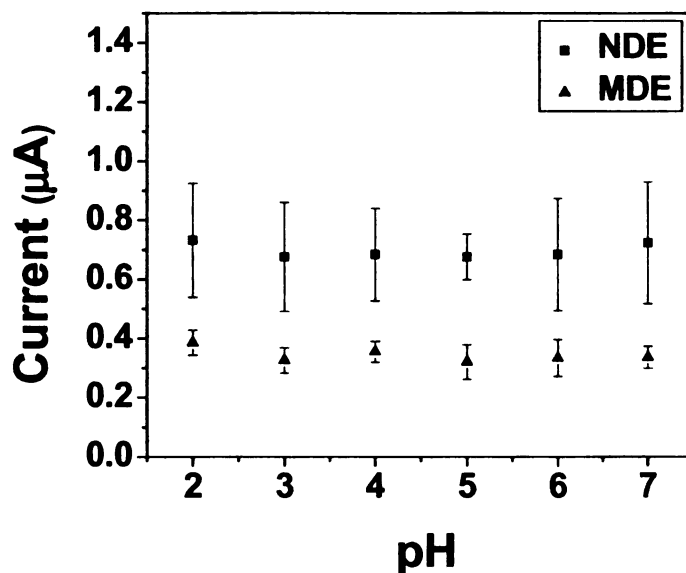


**Figure 3.4.** Background current at 500 mV vs. Ag/AgCl for BND and BMD as a function of the solution pH. Electrolyte = 50 mM phosphate buffer. Scan rate = 100 mV/s. Electrode geometric area = 0.20 cm<sup>2</sup>. Error bars represent the

standard deviation of the background current for 3 electrodes of each type (n = 3).

Cyclic voltammetric i-E curves for NE were next collected at each pH using both BND and BMD. The electrochemical behavior of catecholamines at various carbon electrodes (i.e., glassy carbon and carbon paste) has been reported on extensively.<sup>[32-34]</sup> At acidic pH, NE is oxidized to noradrenoquinone (NE-quinone) via a 2-electron, 2-proton quasi-reversible redox reaction, as shown in Figure 3.5. Another possible redox reaction is shown in Figure 3.6 that involves nucleophilic attack by the side-chain amine to form an indole. Under acidic conditions, the amine group is protonated, which eliminates any possible cyclization of the NE-quinone via the side-chain attack.<sup>[32]</sup> The BND and BMD i-E curves shown in Figures 3.8 and 3.9 were all background corrected. Figure 3.8 (pH 2) shows a cyclic voltammetric i-E curve for NE at pH 2. The arrow depicts the scan direction. Peak (1) is the oxidation of protonated NE to NE-quinone and peak (2) is the reduction of the product and regeneration of the protonated NE.

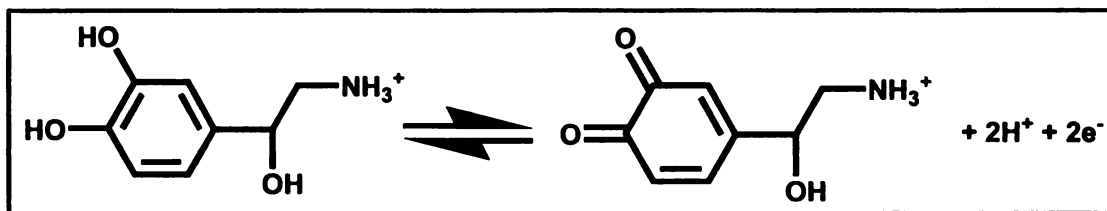


**Figure 3.5.** The reversible electrochemical oxidation of NE to noradrenoquinone (NE-quinone).

At neutral pH, the electrochemistry of NE is more complex. With increasing pH, the reversibility of most hydroquinone/quinone and catechol type systems decrease and the second redox couple becomes more prominent.<sup>[35]</sup> In CV's for NE at pH 2 - 4, the predominant redox couple at both electrodes is the 2-proton, 2-electron redox reaction of NE converting to noradrenoquinone, as shown in Figure 3.5. However, at pH greater than 4, another set of peaks develop between -0.4 and 0.1 V, evidence that another redox reaction is taking place. These new peaks are attributed to the redox couple, shown in Figure 3.6. As the pH increases, the second set of peaks become more intense and the reduction peak for the NE-quinone is dramatically suppressed, as seen in Figures 3.8 and 3.9. This trend is similar to that found in the literature and was attributed to a follow-up ECE process in which the generated NE-quinone oxidizes leuconoradrenochrome which then regenerates NE.<sup>[33, 35]</sup>

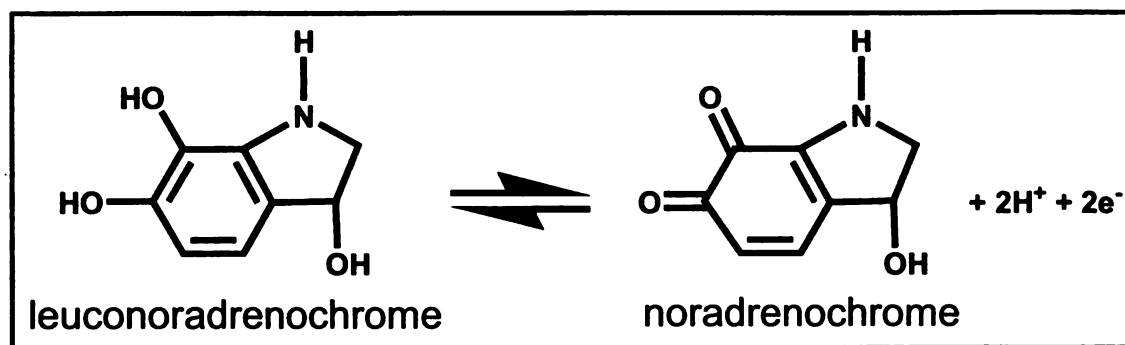


**Figure 3.6.** Cyclized NE observed at higher pH (>4). This is the reversible reaction for peaks 3 and 4.

With increasing pH, the amount of protonated NE and produced NE-quinone in solution decreases,<sup>[36]</sup> as evidenced in Figures 3.8 and 3.9 by the decreasing  $i_p^a$  of peak 1 which corresponds to the oxidation of NE to NE-quinone. The unprotonated NE-quinone, present at higher pH, is a highly reactive species susceptible to nucleophilic attack at the 6-position on the aromatic ring by the side-chain amine. The irreversible intramolecular 1,4 Michael addition occurs forming leucoadrenochrome, Figures 3.6 and 3.7.<sup>[27, 35, 37-39]</sup> Leucoadrenochrome (peak 4) is more easily oxidized than the starting NE (peak 1), and is observed in the following i-E curves recorded for NE at both BND and BMD in buffer with pH > 4.<sup>[35, 38, 39]</sup> The noradrenochrome is reduced during the negative scan, which then forms leucoadrenochrome.

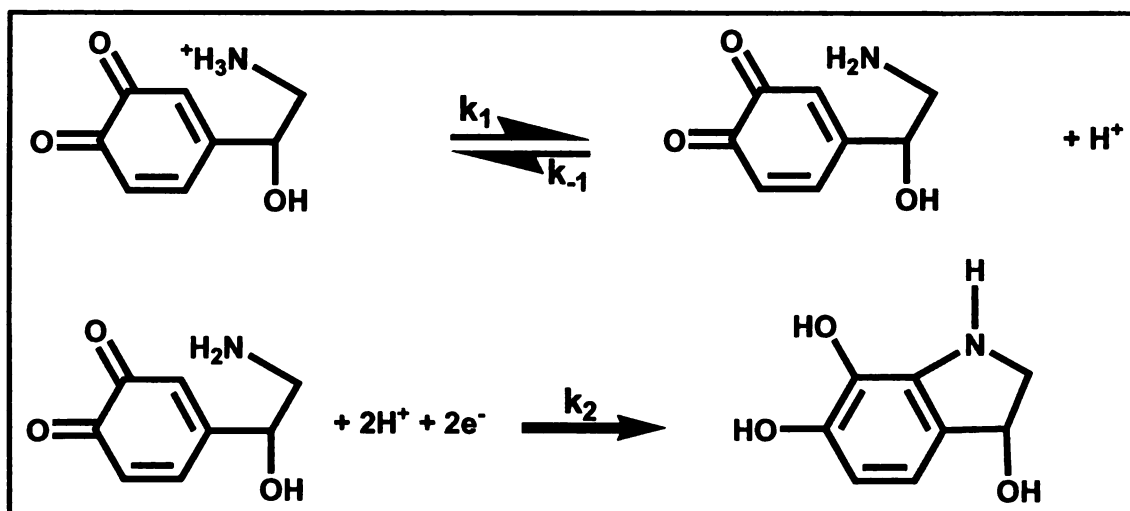


**Figure 3.7.** Intramolecular cyclization of the protonated NE-quinone.<sup>[39, 40]</sup>

The CV i-E curve is interpreted as reflecting the contribution of two redox systems, with corresponding peaks for the NE/NE-quinone and leucoadrenochrome/noradrenochrome redox couples. These results are similar

to those described previously in CV studies of L-dopa and epinephrine at various pH.<sup>[36, 40, 41]</sup> For example in Figure 3.8 (pH 6), the CV begins at a potential of 0 V and is scanned positive. The peak (4) is attributed to the oxidation of leuconoradrenochrome to noradrenochrome (the mechanism depicted Figure 3.6) followed by a peak (1) where NE is oxidized to NE-quinone (the mechanism shown in Figure 3.5). The first peak of the reductive scan, (2), corresponds to the reaction of NE-quinone to NE followed by noradrenochrome (A-NE) back to leuconoradrenochrome at a more negative potential, peak (3).<sup>[33, 35, 39]</sup>

Another observation is the greater  $i_p^{ox}$  on BND than on BMD for NE at all pH. This could be due to some preconcentration of the analyte on the former surface due to adsorption. This issue will be addressed further below. BND has a higher fraction of boundary where  $sp^2$  bonded carbon resides. This finding also leads to speculation that BND exhibits greater adsorption than BMD.<sup>[6, 11]</sup>

The CV i-E curves for NE in phosphate buffer at pH 7 illustrate that leuconoradrenochrome (LA-NE) is not present in solution during the first positive-going sweep of the scan. This is revealed in Figures 3.8 and 3.9 (pH 7). The BND reveals a small peak corresponding to the LA-NE species on the first sweep. The peak for LA-NE is of lesser intensity than the following scans, which demonstrate the generation of LA-NE and the corresponding A-NE with each successive scan. This particular trend was also observed for NE at a glassy carbon electrode in phosphate buffer saline, pH 7.4.<sup>[42]</sup>

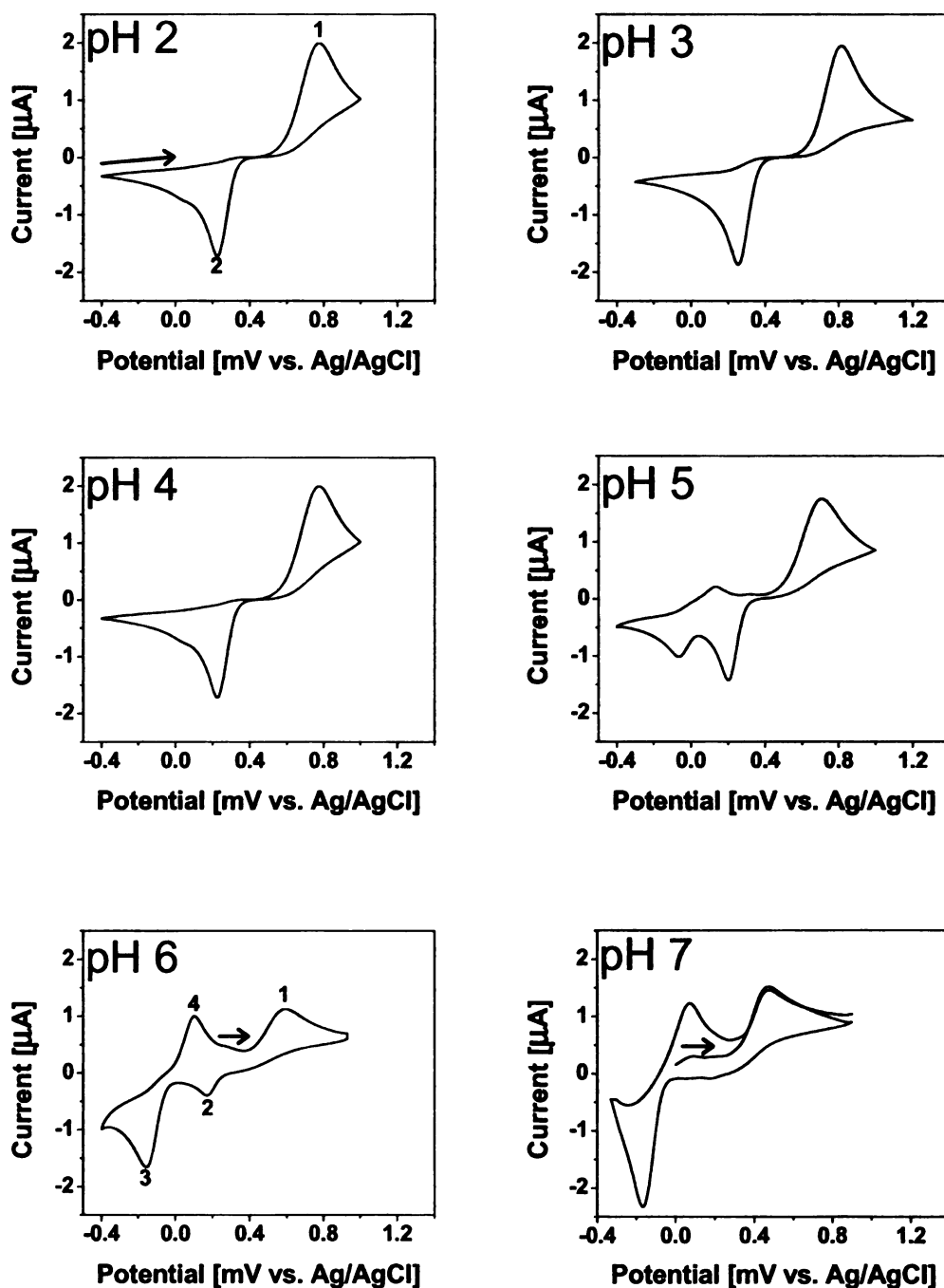


**Figure 3.8.** Cyclic voltammetric i-E curves for 25  $\mu\text{M}$  NE in 50 mM phosphate buffer at various pH. Detection electrode = BMD. Scan rate = 100 mV/s. Electrode geometric area = 0.2  $\text{cm}^2$ . Scans 9-10 shown for pH 2-6, scans 1-3 shown for pH 7.

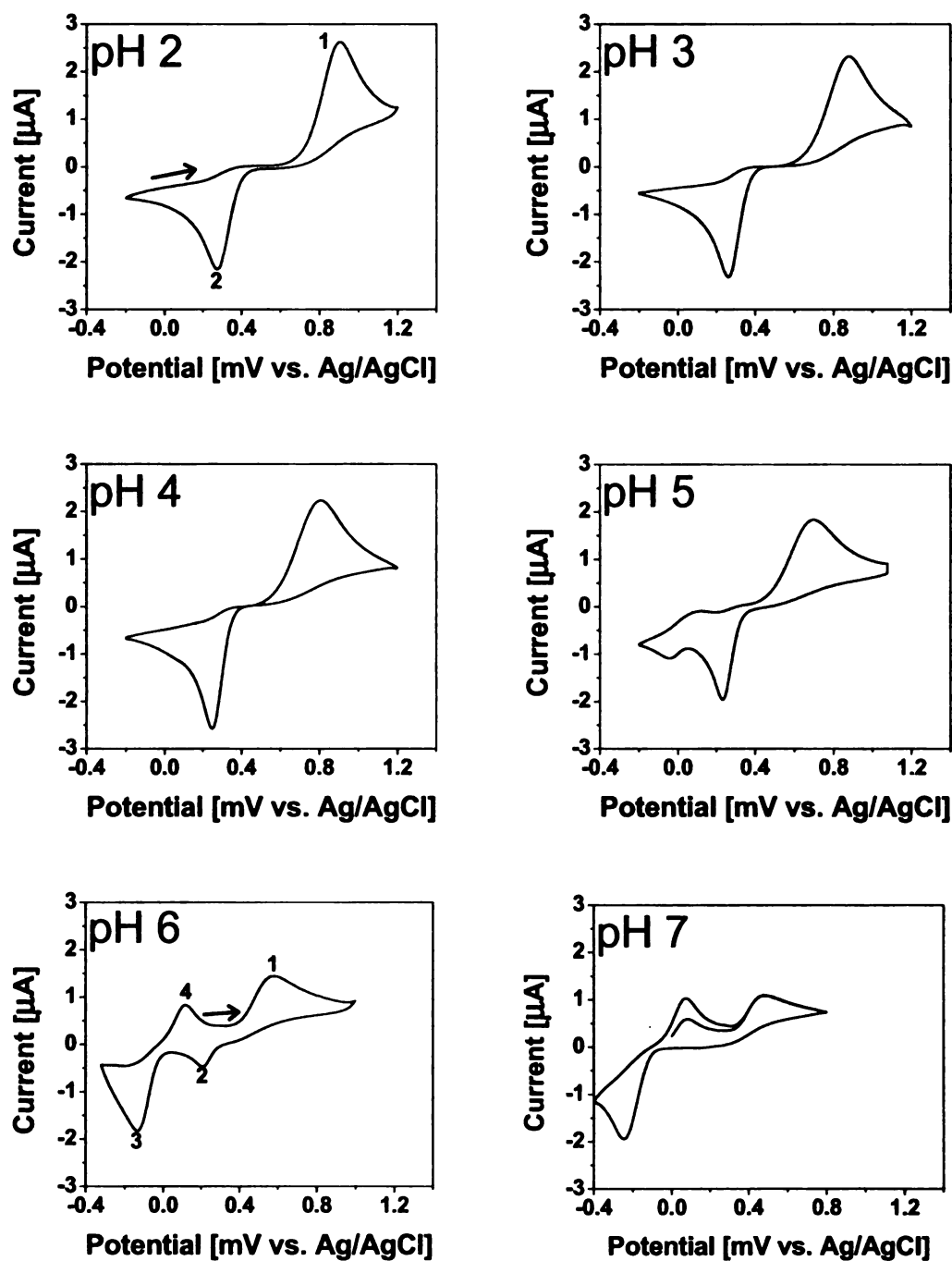


**Figure 3.9.** Cyclic voltammetric i-E curves for 25  $\mu\text{M}$  NE in 50 mM phosphate buffer at various pH. Detection electrode = BND. Scan rate = 100 mV/s. Electrode geometric area = 0.2  $\text{cm}^2$ . Scans 9-10 shown for pH 2-6, scans 1-3 shown for pH 7.

Cyclic voltammetric i-E curves of 25  $\mu\text{M}$  NE in phosphate buffer, pH 7.2, were recorded as a function of scan rate. The series of curves are shown in Figure 3.10. The cyclic voltammograms revealed a peak for the reduction of NE-quinone to NE at scan rates  $\geq 300$  mV/s. The peak increases with increasing scan rate. This observation is likely due to the reduction of NE-quinone before it cyclizes or oxidizes LA-NE in a follow-up reaction through a complex ECE/ECC mechanism described by Hawley and Adams.<sup>[32, 33, 35]</sup> The potential of the anodic peak corresponding to the oxidation of NE shifts positive with increasing scan rate evidence of a quasi-reversible process.<sup>[42]</sup> The anodic peak current for the oxidation of NE increases as a function of the scan rate indicative of diffusion-limited reaction kinetics ( $r^2 > 0.99$ ).

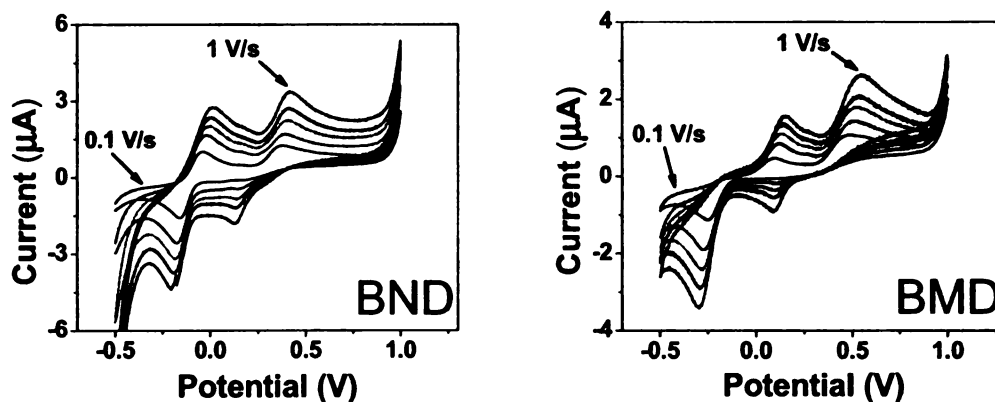


**Figure 3.10.** i-E curves for 25  $\mu\text{M}$  NE in 0.1 M phosphate buffer (pH 7.2) recorded as a function of scan rate. Scan rates 100, 300, 500, 700 and 1000 mV/s. Scans 9-10 shown. All i-E curves are background corrected.

The relationship between the NE oxidation peak current and the scan rate was also probed in 25  $\mu\text{M}$  NE in phosphate buffer, pH 2. The i-E curves were

recorded at rates of 50 mV/s to 500 mV/s for 5 cycles. The oxidation peak current (peak 1) was plotted versus the square root of the scan rate ( $v^{1/2}$ ) for both a BMD and a BND. Figure 3.11, illustrates the linear dependence of  $i_p$  with  $v^{1/2}$ . Both plots had  $r^2$  values of  $>0.99$ . The linearity indicates that the rate of the reaction is diffusion controlled. The theoretical plot is calculated for a 2-electron process by the Randles-Sevcik equation defined in section 3.2. With increasing scan rate, a deviation from ideal behavior is observed. This may be a result of an electroactive area less than the geometric area of the electrode defined by the o-ring. A calculation of the area as a function of the slope for  $i_p$  vs.  $v^{1/2}$  on BND and BMD, results in areas of  $0.12 \text{ cm}^2$ , which is different from the  $0.20 \text{ cm}^2$  calculated from the radius of the o-ring. The discrepancy between the measured and theoretical slopes is attributed to a true area that is less than the geometric area. The non-zero intercepts for both BND and BMD lead to further speculation that this is the case.

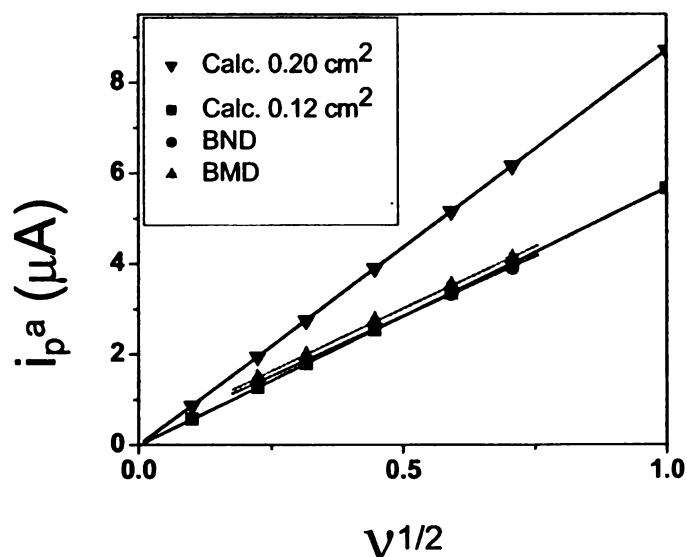


**Figure 3.11.** Dependence of peak oxidation current ( $i_p$ ) on square root of the scan rate ( $v$ ) at BMD and BND in 25  $\mu$ M NE. Electrolyte = 50 mM phosphate buffer, pH 2. BMD  $r^2 = 0.99$  ; BND  $r^2 = 0.99$ . Electrode area = 0.2  $\text{cm}^2$ , reference electrode = Ag/AgCl. 0.20  $\text{cm}^2$ ,  $y = 8.70x$ ; 0.13  $\text{cm}^2$ ,  $y = 5.67x$ ; BND,  $y = 5.30x + 0.20$ ; BMD,  $y = 5.50x + 0.25$ .

Figure 3.12 is a plot of the anodic peak current for the oxidation of NE at BMD and BND plotted with respect to the pH of the electrolyte. The dotted line represents the theoretical current of 2.58  $\mu$ A, calculated using the Randles-Sevcik equation described previously. Observed is that both the electrodes demonstrate current comparable with the theoretically derived value for a system where the reaction rate is limited by semi-infinite linear diffusion of the reactant species to the electrode surface. The average current values for the BND electrodes are slightly higher than those for BMD. The diffusion coefficient for NE used in the calculations was  $5.5 \times 10^{-6}$   $\text{cm}^2/\text{s}$ .<sup>[43]</sup> As the pH increased the anodic peak current decreased. At low pH, unprotonated NE is present at infinitesimal concentrations; however, as the pH is increased, the concentration of the unprotonated species increases.<sup>[37, 42]</sup>

The decrease in oxidation current may be directly related to the cyclization of the unprotonated NE, thus decreasing the NE available for oxidation. This trend is similar to what has been published for NE as a function of pH on another carbon electrode.<sup>[44]</sup> Chen et. al. observed decreasing  $i_p$  with increasing pH, much like what was observed with BND, using a modified glassy carbon electrode. In their measurements, the current was stable until pH 4 after which it

diminished steadily to pH 7.<sup>[44]</sup> Using a carbon paste electrode, Hawley observed a broadened anodic peak accompanied by decreasing current as pH was increased, much like what was observed in these measurements.<sup>[33]</sup>

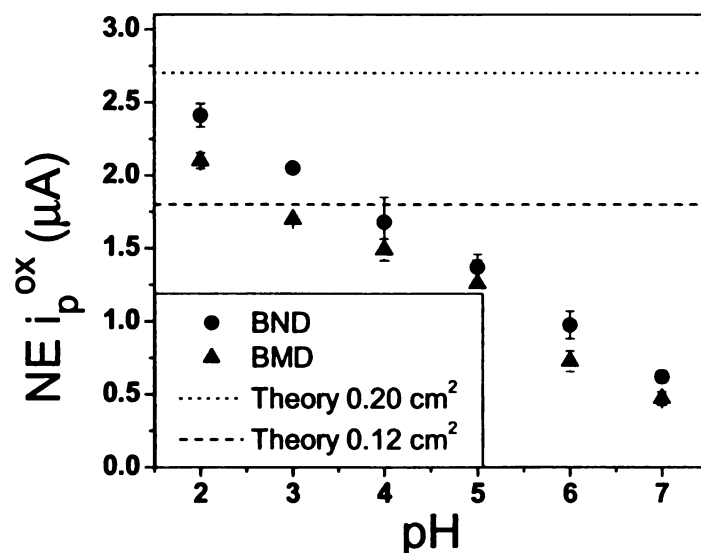


**Figure 3.12.** A plot of peak anodic current for 25  $\mu\text{M}$  NE at BMD and BND as a function of solution pH. Electrolyte = 50 mM phosphate buffer. Electrode area =  $0.2\text{ cm}^2$ , reference electrode = Ag/AgCl. Scan rate = 100 mV/s.

Next, a plot of the peak potential for the oxidation of NE was plotted as a function of pH, Figure, 3.13; this type of plot is often used to study the kinetics of electrochemical reactions. The  $E_p^{\text{ox}}$  reflects the ease of the oxidative process, for example, a high  $E_p^{\text{ox}}$  means that a large overpotential is required to drive the electron-transfer across the solution/electrode interface. The plot shows the negative shift of the peak potential with increasing pH. The shift of  $E_p^{\text{ox}}$  with pH is expected due to the involvement of protons in the redox reaction. This observation was seen by other groups studying NE at glassy carbon and carbon

paste electrodes.<sup>[40, 45]</sup> Another observation is that oxidation of NE at the BND requires a larger driving force ( $\approx 60$  mV) than the BMD. For the anodic peak, the slopes of these curves are  $-41$  and  $-33$  mV/pH between pH 2-4 for the BND and BMD respectively, the slope then increases to  $-117$  and  $-103$  mV/pH for pH 4-7. The cathodic peak for BND and BMD is much less dependent on pH with slopes of  $-15$  and  $-23$  mV/pH, respectively. This observation, that the anodic process has greater pH dependence than the cathodic one has been described by Wightman and is characteristic of catechols in aqueous solution.<sup>[46]</sup>

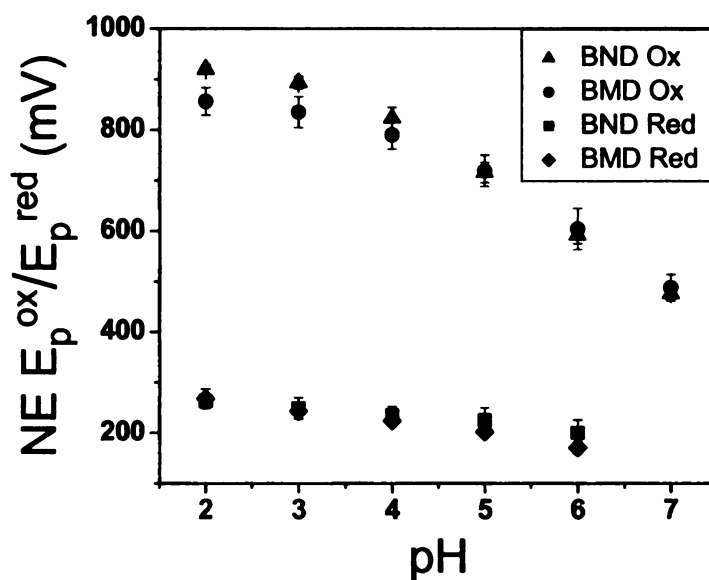


**Figure 3.13.** A plot of peak potential for  $25 \mu\text{M}$  NE at BMD and BND as a function of solution pH. Electrolyte =  $50 \text{ mM}$  phosphate buffer. Electrode area =  $0.2 \text{ cm}^2$ . Reference electrode = Ag/AgCl.

The peak separation,  $\Delta E_p$ , for the oxidation and reduction potentials of NE were next studied.  $\Delta E_p$ , related to the heterogeneous rate constant, allows for

the assessment of the reaction kinetics of a particular system if ohmic losses can be corrected for. The narrow  $\Delta E_p$  for systems such as  $\text{Fe}(\text{CN})_6^{-3/4}$  and  $\text{Ru}(\text{NH}_3)_6^{+3/+2}$  reflects relatively rapid reaction kinetics close to the theoretically expected value.<sup>[9]</sup> For NE, on the other hand, a large  $\Delta E_p$  is observed for both BMD and BND, however, this is an expected outcome for a catecholamine on diamond.<sup>[4, 10, 16, 31]</sup> The non-polar, hydrogen-terminated diamond electrode surface is a substrate which catechols do not adsorb to readily, it lacks carbon-oxygen functionalities and has only a small degree of non-diamond  $\text{sp}^2$  carbon impurity.<sup>[16]</sup> Rapid electron-transfer kinetics are observed for catechols at  $\text{sp}^2$  carbon electrodes due to a mechanism of self-catalysis. Inhibition of the adsorption of the analytes for self-catalysis thus inhibits the electrode kinetics and a large  $\Delta E_p$  is observed.<sup>[4, 16, 47-49]</sup>

Another observation is that with increasing pH, there is a decrease in the  $\Delta E_p$ . Although the slopes of the data do not reveal any obvious trend, some speculation can be made. The hydrogen-terminated diamond electrodes are chemically inert and they are minimally affected by solution pH due to the absence of ionizable surface oxides.<sup>[16]</sup> Therefore, the trend observed for the  $\Delta E_p$  for NE at BMD and BND may be due to electrostatic repulsion of any positively charged carbon-oxygen functionalities and protonated NE at low pH.<sup>[49]</sup> As the pH is increased, NE becomes unprotonated and faster reaction-kinetics are observed at the electrode interface.

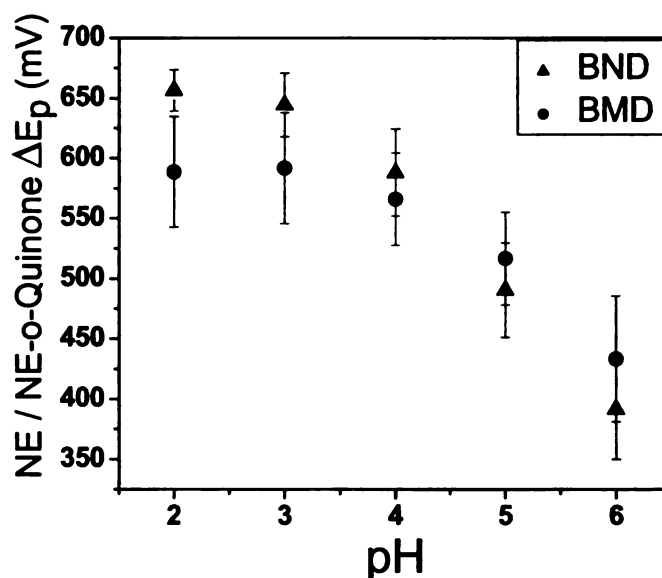


**Figure 3.14.** Plots of  $\Delta E_p$  ( $E_p^{ox} - E_p^{red}$ ) for 25  $\mu\text{M}$  NE at BMD and BND as a function of solution pH. Electrolyte = 50 mM phosphate buffer, pH 2. Electrode area = 0.2  $\text{cm}^2$ , reference electrode = Ag/AgCl.

Even though both BMD and BND exhibit similar electrochemical qualities such as the magnitude of the analytical signal and the response stability, BND was selected for use in the catecholamine analysis work discussed in the next chapter. This decision was guided, in part, by previous work from our group in which BND exhibited superior detection figures of merit as compared to BMD.<sup>[6]</sup>

### 3.4 Measurement of NE Adsorption on BDD

The following experiments conducted were to determine whether NE adsorbs onto the surface of BDD electrodes. It was speculated that the polar NE

has low affinity for the hydrogen-terminated surface of the diamond. This is what renders diamond resistant to fouling by polar adsorbates, such as catecholamines. Evidence for this was shown with species, such as anthraquinonedisulfonate. In this study, BDD was compared with three other carbon electrode materials (highly oriented pyrolytic graphite, GC and hydrogenated-GC) and it was found that negligible adsorption occurred on diamond.<sup>[50]</sup>

Chronocoulometry (CC) involves the measurement of charge (coulombs) as a function of time in response to an applied potential. CC is a technique useful for the determination of adsorbed electroactive species on an electrode surface. For CC studies, a double-potential step waveform was used where  $E_1 = -0.5$  V and  $E_2 = 0.8$  V for GC and  $E_2$  for diamond was 1V. The potentials were chosen from cyclic voltammetric i-E curves.  $E_1$  was taken as an area where no faradaic current was generated;  $E_2$  was taken from an area of the i-E curve where faradaic current was mass-transfer limited. The total charge ( $Q_t$ ) passes originates from three sources; double-layer charging ( $Q_{DL}$ ), electrolysis of analyte in solution ( $Q_f$ ) and electrolysis of surface bound species ( $Q_{ads}$ ). The expression is written as follows:

$$Q_{Total} = Q_F + Q_{DL} + Q_{ADS}$$

$$Q_F = 2nFAD^{1/2}Ct^{1/2}\pi^{-1/2}$$

$$Q_{ADS} = nFA\Gamma^0$$

As can be seen, the charge due to the adsorbed species does not have a time dependence, therefore it can be distinguished from the charge due to the electrolysis of solution species. The surface-bound species is immediately

electrolyzed whereas the species in solution must diffuse to the electrode surface to be electrolyzed.<sup>[51]</sup> Figure 3.15 shows three chronocoulograms, one for GC, BND and BMD. The GC coulogram is provided for comparative purposes. GC exhibits evidence of adsorption of NE due to the difference in the y-axis intercept for the  $Q_f$  and  $Q_{DL}$  vs.  $t^{1/2}$  plots. The difference in y-axis intercept is due to the charge passed to oxidize adsorbed NE. The charge equal to the surface coverage according to the relationship  $Q_{ADS} = nFA\Gamma^\circ$ . The surface coverage determined by the plot provided is  $\Gamma^\circ = 21 \text{ pmol/cm}^2$ . However, there is no evidence for adsorption at either BND or BMD. Three electrodes of each BDD type were analyzed for adsorption by CC.

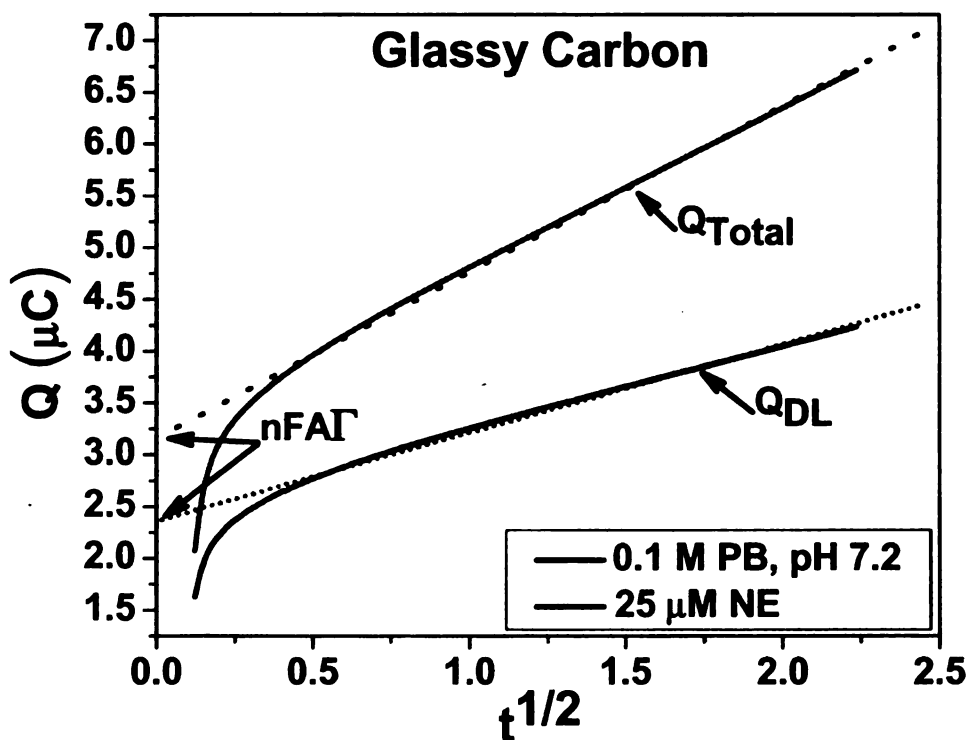


**Figure 3.15.** Chronocoulogram of 25  $\mu\text{M}$  NE at freshly polished GC. Electrolyte = 100 mM phosphate buffer, pH 7.2. Electrode area = 0.2  $\text{cm}^2$ . Reference

electrode = Ag/AgCl. A 5-second double-potential step waveform was used where  $E_1 = -0.5$  V,  $E_2 = 0.8$  V.

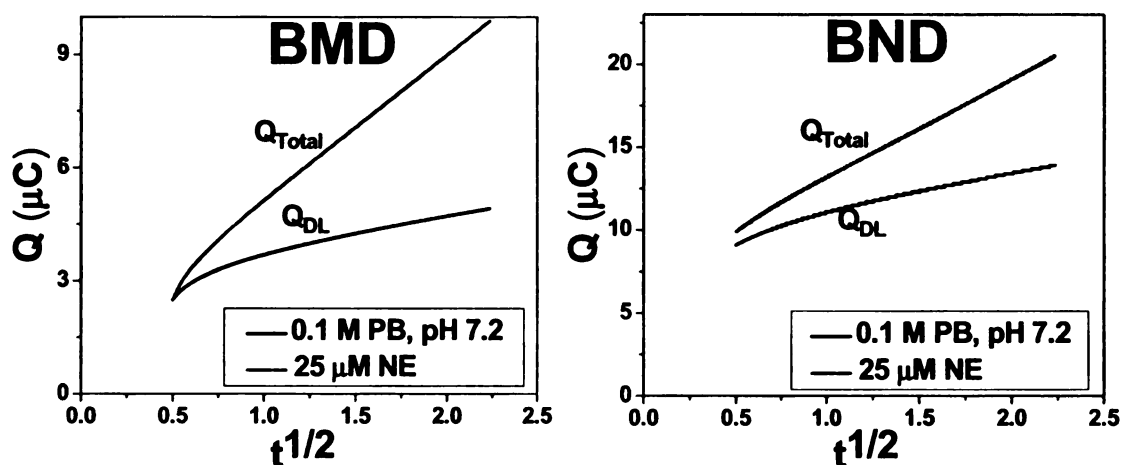


**Figure 3.16.** Chronocoulograms of 25  $\mu$ M NE at BND and BMD. Electrolyte = 100 mM phosphate buffer, pH 7.2. Electrode area = 0.2 cm<sup>2</sup>. Reference electrode = Ag/AgCl. A 5-second double-potential step waveform was used where  $E_1 = -0.5$  V,  $E_2 = 1$  V.

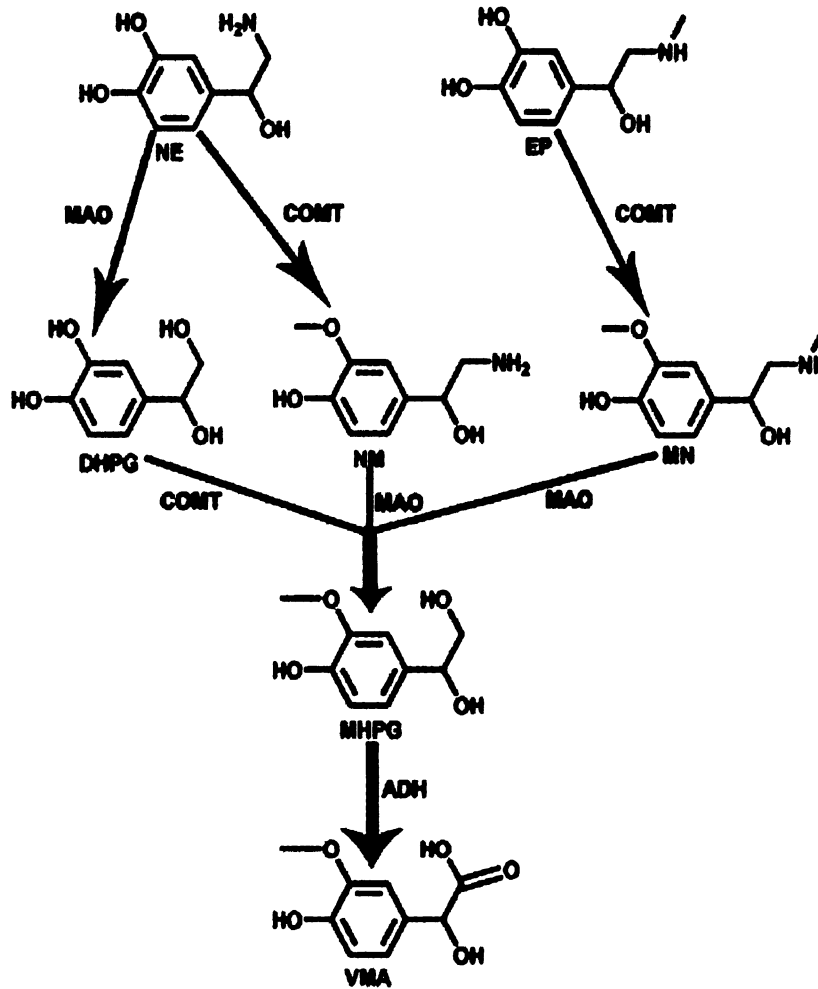
To verify the CC results semiintegral analysis and log-log plots were performed. Log-log plots of anodic peak current as a function of scan rate ( $\log i_p$  vs  $\log v$ ) revealed slopes of 0.49 and 0.48 for BND and BMD respectively. In the case of weak adsorption, the slope would be expected to lie between 0.5 and 1.0, where 0.5 is characteristic of diffusion-controlled processes and 1.0 is expected for processes entirely due to adsorption.<sup>[52]</sup> Semiintegral analysis of the anodic peak revealed a sigmoidal curve with no evidence of adsorptive current for both BMD and BND in support of the previous coulometric data.<sup>[52, 53]</sup> Semiintegral analysis of the anodic peak for GC however revealed a peaked sigmoidal curve evidence for adsorption of NE<sup>[52]</sup>, also in support of the coulometric results.

## **Chapter 4**

### **Determination of Norepinephrine in Normal, Sham, DOCA-salt and 6-Hydroxydopamine treated Rat Tissue by Reversed-Phase HPLC Separation and Amperometric Detection using a Boron-Doped Nanocrystalline Diamond Thin-Film Electrode**

#### **4.1 Introduction**

Catecholamines and their metabolic products are of great importance as potential biomarkers for neurological disorders and certain physiological diseases.<sup>[54]</sup> Figure 4.1 is a modified schematic, originally published by Eisenhoffer, illustrating the various pathways for metabolism of norepinephrine and epinephrine derived from the sympathoneuronal and adrenalmedullary sources.<sup>[55]</sup> The studies presented herein primarily focus on the role of norepinephrine (NE) in the sympathetic nervous system (SNS). The SNS is recognized as the “fight or flight” system and is responsible for physiological responses, such as bronchodilation, cardiac acceleration, and inhibition of digestion.<sup>[56]</sup>



Abbreviations: NE, norepinephrine; EP, epinephrine; DHPG, 3,4-dihydroxyphenylethylglycol; MN, metanephrine; NM, normetanephrine; MHPG, 3-methoxy-4-hydroxyphenylethylene glycol; VMA, vanillylmandelic acid; MAO, monoamine oxidase; COMT, catechol-O-methyltransferase; and ADH, alcohol dehydrogenase.

**Figure 4.1.** Norepinephrine and epinephrine metabolic pathways.

Each of the species in the metabolic pathway has the potential of eliciting information about regulatory systems as well as disease states. Monitoring each of these chemicals simultaneously would be ideal in order to further develop a

picture of the SNS and its functional changes in disease. The sympathoneuronal metabolic pathway describes NE and EP, how each is metabolized in the sympathetic nervous system, and thus their relationship to one another. The chemical complexity of the matrices associated with the analysis of catecholamines in tissue and bodily fluids, as well as the presence of thousands of other compounds, necessitates that a suitable means of target analyte separation and detection be available.<sup>[54, 57]</sup> Many methods have been developed for this type of analysis including gas-chromatography/mass spectrometry (GC-MS), radioenzymatic methods, and high-performance liquid chromatography (HPLC) coupled to fluorescence (HPLC-FD), UV or electrochemical detection (HPLC-EC).

HPLC-EC was used in this work in order to take advantage of the excellent properties of diamond electrodes. Unlike GC-MS and HPLC coupled with fluorescence detection (FD), HPLC-EC requires no lengthy derivatization step prior to analysis.<sup>[23, 58]</sup> Catecholamines can be detected directly by their native fluorescent properties using FD ( $\lambda_{\text{ex}} = 275 \text{ nm}$ ,  $\lambda_{\text{det}} = 320\text{-}350 \text{ nm}$ )<sup>[59]</sup> but it requires a high-intensity excitation source, such as an Ar or Kr ion laser, which may also excite a number of potentially interfering compounds.<sup>[1, 54, 59, 60]</sup> ECD has been shown to afford superior detection figures of merit compared to FD for catecholamines.<sup>[61, 62]</sup> However, recent groups have demonstrated the ability of FD to meet comparable sensitivities for detection of catecholamines which EC boasts.<sup>[1, 59]</sup> UV detection, on the other hand lacks the sensitivity and selectivity required for the analysis of biogenic amines derived from plasma or tissue.<sup>[6, 60]</sup>

The HPLC-EC method for the qualifying and quantifying in bodily fluid and tissue was first reported in 1973. Today, it remains the method of choice for this type analysis due to a relatively low cost, good sensitivity, selectivity and reproducibility as well as the catecholamines' ease of oxidation.<sup>[20, 23, 32, 33, 63]</sup>

This chapter applies the novel BND electrode discussed in Chapter 3 in the electrochemical detection with RP-HPLC separation. The optimization of the separation and detection conditions is described first. This is followed by a discussion of the application of the method for the determination of NE from various rat tissues.

## 4.2 Development of the Method for Neurogenic Amine Standards

The most common column used for separating catecholamines is an octadecylsilica (C-18) type.<sup>[20, 64]</sup> In RP-HPLC, the retention of compounds is described by the solvophobic theory.<sup>[65]</sup> Catecholamines are small, polar compounds, thus, in RP-HPLC, these compounds elute rapidly from the column with a poor separation. To overcome this problem, it is common that an ion-pairing agent is added to the mobile phase to enhance their retention by giving the molecule more non-polar character.<sup>[58, 66]</sup>

Multiple mobile phase compositions have been used to separate catechols and catecholamines. For the most part, the mobile phase consists of an organic modifier, an ion-pairing agent, EDTA, and a buffering system, such as

phosphate/citrate buffer.<sup>[22, 66-69]</sup> These complex mobile phases suffer from laborious, time-consuming preparation steps and at times lack of separation reproducibility.<sup>[58, 63]</sup> Table 4.1 lists examples of mobile phases and columns used to separate catecholamines and metabolites from tissue and bodily fluids.

**Table 4.1.** Selected examples of mobile phase composition and column type for catecholamine analysis.

Mobile Phase Composition	Column Type	pH	Run (min)	# Solute
0.05 M Sodium Dihydrogen Phosphate, 0.03 M Citric acid, 0.1 M EDTA, 0.042% SOS, 25% MeOH <sup>[66]</sup>	ODS 250 x 4.6 mm	2.75	13	8
0.1 M Potassium Dihydrogen Phosphate, 0.5 mM OSA, 9% ACN <sup>[22]</sup>	ODS 150 x 4.6 mm	4.75	16	5
0.1 M Sodium Acetate, 0.2 M Citric Acid, 0.2 mM EDTA, 0.4 mM SOS, 4.5% MeOH <sup>[67]</sup>	ODS 250 x 4.6 mm	4.85	>30	4

OSA – octane sulfonic acid, SOS – sodium octyl sulfate, EDTA – disodium ethylenediamine triacetate

It was our desire to achieve a separation of catecholamines using an isocratic mobile phase. Isocratic elution uses a constant mobile phase composition and thus requires less time in between injections for equilibration, minimizing solvent waste and analysis time. Gradient elution consumes significant quantities of mobile phase during reequilibration between each run,

which makes this method more wasteful and time-consuming than an isocratic separation. Gradient elution can be beneficial for the separation of complex mixtures, however, when using the method for multiple injections and high through-put, such as for use with an autoinjector, an isocratic separation may be better suited for the task.

The method described herein is an attempt to devise a RP-HPLC-EC method utilizing a boron-doped diamond thin-film as the working electrode and an analytical column with a novel stationary phase. A Supelco Discovery HS-F5 analytical column was tested for the ability to separate the catecholamines and metabolites. This column is a reversed-phase, silica-based type, like the C-18 columns; however, it has pentafluorophenyl functional groups bound to the support material via an alkyl linker. The stationary phase of this column is exceptional for separation of small polar, aromatic, compounds, such as catecholamines.<sup>[58, 70, 71]</sup>

Retention of catecholamines on the pentafluorophenyl stationary phase can occur by several types of interactions including  $\pi$ - $\pi$ , electrostatic, charge-transfer, and hydrogen-bonding.<sup>[70, 71]</sup>

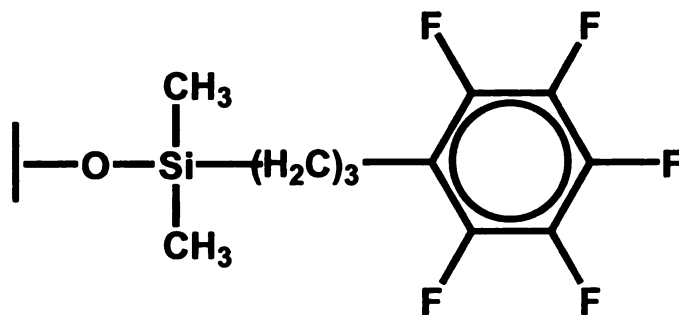


**Figure 4.2.** The chemical composition of the Supelco Discovery HS-F5 stationary phase.

Besides the enhanced retention of small, polar molecules on this column, another benefit is that the column is safe to use with a fully aqueous mobile phase without performance loss or compromise of its chemical stability.<sup>[58]</sup> The mobile phase that was used for the following separations was a 50 mM ammonium formate solution in doubly deionized water, adjusted to pH 3 with concentrated formic acid. This simple mobile phase could be prepared quickly. The formate buffer was used at pH 3, the optimal pH for separation of catecholamines in this buffer.

Catecholamine standards were prepared in 10 mM stock solutions with 5 mM metabisulfite aided as an antioxidant. This prevents the formation of oxidative degradation products.<sup>[20]</sup> Dilution of the stock solutions with ammonium formate buffer or deionized water was performed before analysis. Stock solutions were kept in a laboratory freezer, wrapped in foil for approximately 1 month or until a decrease in analyte peak height or additional peaks began to appear in the chromatograms. At this point, the stock solutions were disposed of and fresh ones prepared.

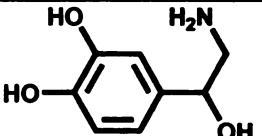
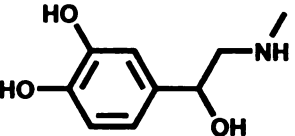
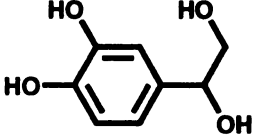
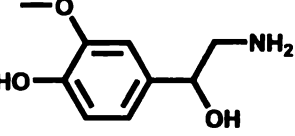
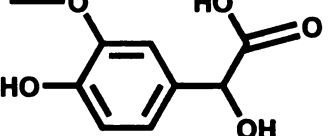
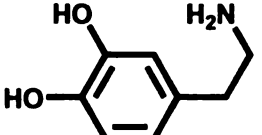
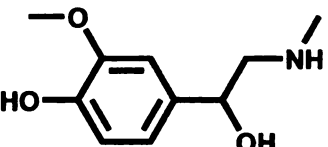
Hydrodynamic voltammetric i-E curves were recorded in order to optimize the detection potential. The oxidation current (detector signal) for the analyte was measured as a function of the applied potential. Figure 4.3 shows a hydrodynamic voltammogram for NE. The curve is sigmoidally shaped with a half-wave potential ( $E^{1/2}$ ) of 840 mV. The limiting current above 1000 mV indicates the rate of the oxidation reaction is controlled by mass transfer. The

magnitude of the background current at each measured potential is denoted in Figure 4.3 by the open circles. The curve shows the increase of the background current with increasing potential of the working electrode. The optimal potential for the detection of NE was determined to be 950 mV, as at this point background current is negligible compared to the large faradaic current for NE oxidation. Similar hydrodynamic voltammograms were obtained for EP, DOPEG, DA, NM, MN and VMA and their respective  $E_{1/2}$  values can be seen in Table 4.2. The structure, molecular weight and  $pK_a$  values for the different solutes studied are listed in Table 4.3.

**Table 4.2.**  $E_{1/2}$  values obtained from hydrodynamic voltammograms for the solutes studied. Detection electrode = BND. Mobile phase was 50 mM ammonium formate buffer (pH 3).

	$E_{1/2}$ (mV)
<b>NE</b>	840
<b>DOPEG</b>	730
<b>EP</b>	850
<b>NM</b>	910
<b>VMA</b>	820
<b>DA</b>	790
<b>MN</b>	920

**Table 4.3.** Molecular structure, molar mass and pK<sub>a</sub> values for catecholamines and related compounds.

	Chemical Structure	pK <sub>a</sub>
<p><b>NE</b> (169.18 g/mol)</p>		8.72, 10.30, 11.69 <sup>[72]</sup>
<p><b>EP</b> (183.20 g/mol)</p>		8.59, 8.65, 9.67, 11.34 <sup>[73]</sup>
<p><b>DOPEG (DHPG)</b> (170.16 g/mol)</p>		9.55
<p><b>NM</b> (183.20 g/mol)</p>		8.25, 9.76
<p><b>VMA</b> (198.17 g/mol)</p>		3.42
<p><b>DA</b> (153.18 g/mol)</p>		9.05, 10.58, 12.07 <sup>[74]</sup>
<p><b>MN</b> (197.23 g/mol)</p>		9.13, 9.76

Molecular structure and pK<sub>a</sub> values of pertinent catecholamines as well as several metabolites. All pK<sub>a</sub> values are calculated by Advanced Chemistry Development software (Solaris, v4.67), except where indicated.

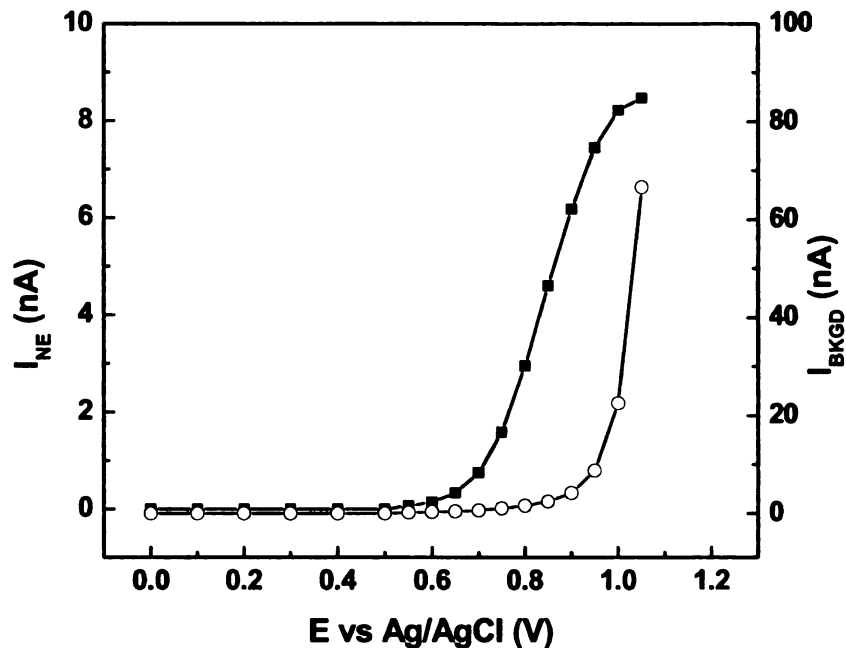


**Figure 4.3.** Hydrodynamic voltammogram obtained for 10  $\mu\text{M}$  NE at BND. ( $\blacksquare$ ) denotes  $I_{\text{NE}}$ , ( $\circ$ ) denotes  $I_{\text{BKGD}}$ . Column = Supelco Discovery HS-F5 (150 mm x 4.6 mm, 5  $\mu\text{m}$ ) equipped with guard column (20 mm x 4.6 mm, 5  $\mu\text{m}$ ). The mobile phase was 50 mM ammonium formate buffer (pH 3). Flow rate = 1 mL/min. Injection volume = 20  $\mu\text{L}$ .

Once the optimum detection potential was determined, the oxidation current as a function of NE concentration was recorded. A typical calibration curve is displayed in Figure 4.4. The BND exhibited a low and stable background current, and a peak-to-peak noise of 60 pA at the detection potential of 0.95 V. For standard solutions, the detector signal changed linearly with the NE concentration ( $r^2 = 0.999$ ) from 0.08 to 1  $\mu\text{M}$ . The limit of quantitation was determined to be 70 nM (S/N = 3) with a sensitivity of 2.5 nA/ $\mu\text{M}$ . These results were comparable to those previously reported by our group.<sup>[6]</sup> Table 4.4 lists the

linear dynamic range, LOQ, sensitivity and RSD for the various compounds separated in the chromatogram, Figure 4.5. Calibration curves for all solutes had  $r^2 \geq 0.99$ .

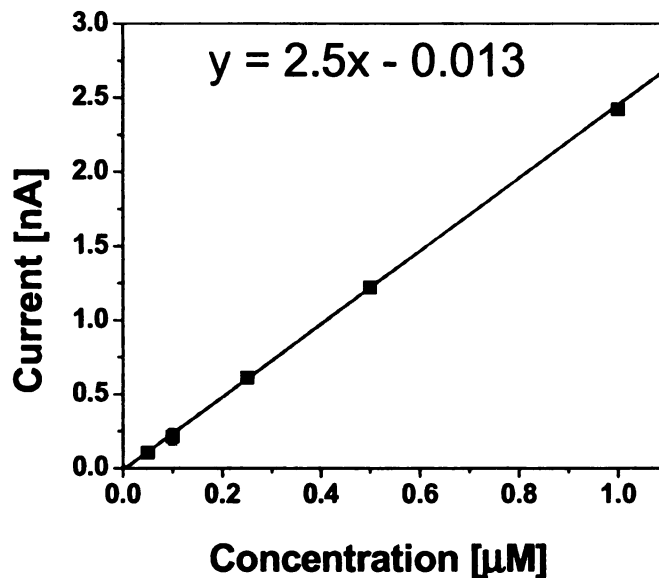


**Figure 4.4.** Response curve for NE at BND.  $R^2 = 0.999$ . The mobile phase was 50 mM ammonium formate buffer (pH 3). Detection potential = 950 mV vs. Ag/AgCl. Flow rate = 1 mL/min.

The retention times of the catecholamines and metabolites were determined by injecting each individual compound. Figure 4.5 displays a chromatogram for a mixture of 3 catecholamines and 4 metabolites. All solutes were adequately separated for quantification. Resolution ( $R_s$ ) of the compounds and their retention times are listed in Table 4.5.

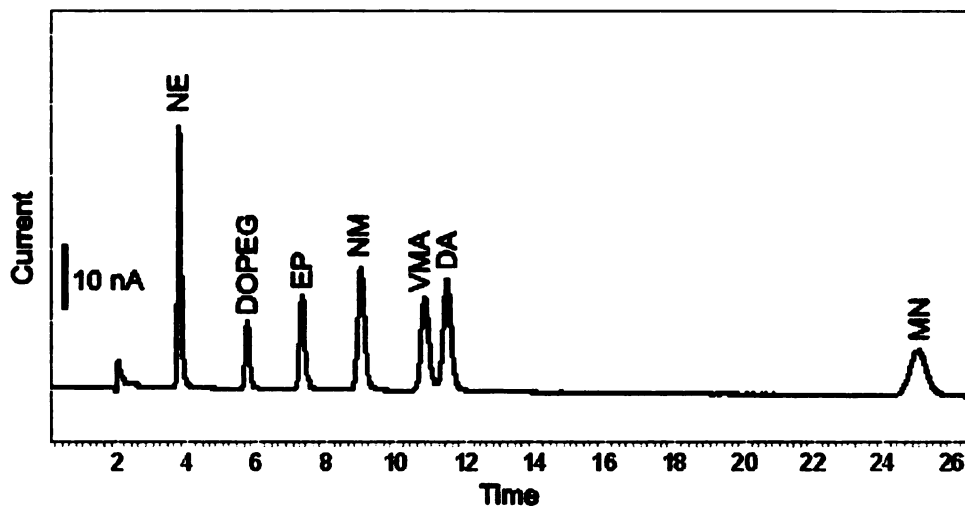


**Figure 4.5.** Chromatogram for several catecholamines (NE, EP, DA) and metabolites (DOPEG, NM, VMA, MN). All solute concentrations were 10  $\mu$ M. Detection electrode = BND. The mobile phase was 50 mM ammonium formate buffer (pH 3). Flow rate = 1 mL/min. Injection volume = 20  $\mu$ L. Detection potential = 950 mV vs. Ag/AgCl.

**Table 4.4.** Figures of merit for the detection of catecholamines by HPLC-EC.

	LDR	Sensitivity (nA/ $\mu$ M)	LOQ	RSD (%)
<b>NE</b>	50 nM – 10 $\mu$ M	2.5	72	1.5
<b>DOPEG</b>	100 nM – 10 $\mu$ M	2.33	77	2.5
<b>EP</b>	100 nM – 10 $\mu$ M	1.41	127	1.8
<b>NM</b>	100 nM – 10 $\mu$ M	0.63	285	2.3
<b>VMA</b>	100 nM – 10 $\mu$ M	2.90	60	2.8
<b>DA</b>	100 nM – 10 $\mu$ M	1.51	118	3.5
<b>MN</b>	500 nM – 10 $\mu$ M	0.25	700	9.0

Detection electrode = BND. The mobile phase was 50 mM ammonium formate buffer (pH 3). Flow rate = 1 mL/min. Injection volume = 20  $\mu$ L. Detection potential = 950 mV vs. Ag/AgCl. RSD was calculated for 1  $\mu$ M concentration of standards (n = 3 injections).

**Table 4.5.** Retention time ( $t_R$ ) and resolution ( $R_s$ ) for various catecholamines and metabolites. The % is the coefficient of variance.

	$t_R$ (min) (RSD)	$R_s$ (RSD)
<b>NE</b>	3.7 ± 0.02%	
<b>DOPEG</b>	5.7 ± 0.04%	5.1 ± 2.3%
<b>EP</b>	7.3 ± 0.05%	3.4 ± 3.8%
<b>NM</b>	8.9 ± 0.03%	3.0 ± 4.5%
<b>VMA</b>	10.8 ± 0.02%	2.9 ± 2.2%
<b>DA</b>	11.4 ± 0.1%	1.0 ± 7.9%
<b>MN</b>	24.9 ± 0.01%	13.3 ± 6.7%

Retention times and resolution values for adjacent eluting solutes determined from the chromatogram. The detection electrode = BND. The mobile phase was 50 mM ammonium formate buffer (pH 3). Flow rate = 1 mL/min. Injection volume = 20  $\mu$ L. Detection potential = 950 mV. n = 4 injections.

The lowest resolution ( $R_s$ ) for the standard mixture was observed between VMA and DA. The background current required approximately 20 min to stabilize to a constant current after detector turn-on. This stabilization time decreased with electrode use. The chromatographic separation of NE, DOPEG, EP, NM, VMA, DA and MN was obtained in reversed-phase mode on a Discovery HS-F5 column. The isocratic separation of the seven solutes took approximately 26 min. The diamond planar thin-film electrode (BND) provided a low and stable background current, with low peak-to-peak noise (~60 pA) at a detection potential of 950 mV.

### 4.3 Application of the HPLC-EC Method for the Quantitation of NE from Tissue

After reproducibly separating and detecting the standard solutions, the method was then applied to the analysis of NE in various types of rat tissue. The research aim was to demonstrate the utility of diamond electrodes for the determination of NE in normal, Sham and DOCA-salt rats. Tissue NE levels are of interest because of the important role of this neurotransmitter in the peripheral sympathetic nervous system. NE is the metabolic precursor to EP and plays a significant role in the regulation blood pressure, as well as other physiological functions. The relationship between NE and other neurogenic amines can be seen in Figure 4.1. NE, and its role in blood pressure regulation, is of particular interest to groups such as ours, who study how the sympathetic nervous system regulates vascular tone.<sup>[75]</sup>

Hypertension is defined as the chronic elevation of blood pressure to levels of 140/90 mm Hg, or greater. Elevated blood pressure causes strain on the heart and vasculature, and can lead to kidney disease, heart disease and stroke. A commonly encountered consequence of hypertension is left ventricular hypertrophy due to the increased stress on the heart. Hypertrophy, or enlargement of the left ventricle, was evident in our hypertensive animals based on the weights of each separated heart chamber.<sup>[75]</sup> Table 4.6 shows the average weight of different sections of the heart from the different test animals used in this work. The pathophysiology of essential hypertension is of particular

concern because in order to better understand the progression of the disease state, one must have a clearer picture of the role of NE in the sympathetic nervous system.

**Table 4.6.** Average weight (n=2) of different heart chambers from the animal models used in this work.

	Normal (g)	SHAM (g)	DOCA (g)	6-OHDA (g)
LA	0.04	0.04	0.04	0.03
RA	0.03	0.05	0.04	0.03
LV	0.59	0.80	0.94	0.54
RV	0.23	0.22	0.22	0.15
VSW	0.19	0.25	0.30	0.15

LA – left atrium, RA – right atrium, LV – left ventricle, RV – right ventricle, VSW – ventricular septal wall. Rat model preparations and definitions can be found in chapter 2.

To fully evaluate the performance of the BND electrode for determination of NE from tissue, development of a practical protocol for the preparation of tissue was first necessary in order to selectively extract NE for analysis. Most electrochemical methods for catecholamine analysis in tissue utilize RP-HPLC for separation by way of a C18 column prior to detection. Amperometric detection is common and is typically performed with a glassy carbon electrode<sup>[22]</sup>.

63, 66, 67, 69, 76-79] . Coulometric detection is also often used these days<sup>[19]</sup>. The mobile phase composition for the separations as mentioned in the previous section consisted of phosphate buffer, EDTA, an ion-pairing agent, and 1-30 % organic modifier maintained at a pH of 2-5. Tissue sample prep found in literature consisted of using either alumina<sup>[19, 63, 76, 78, 80]</sup>, liquid-extraction<sup>[67]</sup>, filtration<sup>[75]</sup> or direct-injection<sup>[69, 77, 79]</sup>. Detection limits for NE were typically in the low pg range.

The specific aim of our work was to develop a sample preparation protocol and a separation method that enables low levels of NE to be detected in various types of tissue. Boron-doped diamond electrodes were used for detection. SPE was used for the selective extraction of NE from tissues with a higher recovery and less laborious work-up than reported commonly used alumina.<sup>[78, 80, 81]</sup> The diamond electrode material is beneficial for this type of analysis since it requires no pretreatment, a wide working-potential range and has a chemically inert surface that is resistant to fouling.<sup>[10, 47, 82]</sup>

#### 4.4 Preparation of Tissue for the Extraction of NE

Organs were quickly removed from the animal and wrapped in aluminum foil, after which they were placed in a freezer (-80 °C) until analysis. For analysis, each sample was placed (while frozen) into a tared 10 mL plastic test tube. The tissue was weighed and a volume of ice-cold perchloric acid (PCA, 0.1

M) was added to the tube. PCA is used to aid in the tissue digestion and denaturation of the proteins.<sup>[18, 19, 24, 62, 69, 76, 83]</sup> Table 4.7 shows the volume of PCA that was added to homogenize each tissue type. These volumes were selected in order to maintain an adequate volume of homogenate supernatant for subsequent solid-phase extraction (SPE). The LA, RA, VSW and RV chambers of the heart had significantly lower masses than the LV. For the aforementioned tissue, an adequate volume for SPE was chosen instead of using a mass/volume ratio as was the case with LV and other tissues.

**Table 4.7.** The volume of PCA to the sample weight for various tissue types analyzed by HPLC-EC.

<b>Tissue</b>	<b>Volume of 0.1 M PCA</b>
Left Atrium	0.9 mL
Right Atrium	0.9 mL
Left Ventricle	2 mL / 0.5 g tissue
Right Ventricle	1 mL
Ventricular Septal Wall	1 mL
Other (Intestine, Spleen, Kidney, Liver)	2 mL / 0.5 g tissue

The tissue was then homogenized for approximately 3 min using a homogenizer, as described in Chapter 2. The homogenate was then carefully transferred to a disposable, capped centrifuge vial and stored on ice until centrifugation. Centrifugation was performed at 4 °C and 13,200 rpm for 15 min.

The vial was then removed and the centrifugate carefully collected with a pipette and transferred to a clean capped vial for cold storage.

#### 4.5 Solid-Phase Extraction (SPE) of Tissue Supernatant

As mentioned previously, tissue homogenate, in which NE and other catecholamines exist, is complex. This makes it difficult to analyze biological samples without some form of sample clean-up. The supernatant from the homogenization procedure was complex containing many compounds that interfered with the detection of NE and other analytes of interest. Direct injection of the homogenate or the supernatant for analysis by HPLC-EC drastically reduced the lifetime of the analytical column and fouled the detection electrode.<sup>[24, 69]</sup> Figure 4.6 shows a chromatogram of an LV supernatant injected after filtration. Based on the retention time for a standard, NE in the tissue cannot be quantified due to the intense interfering peaks present in the biological matrix.

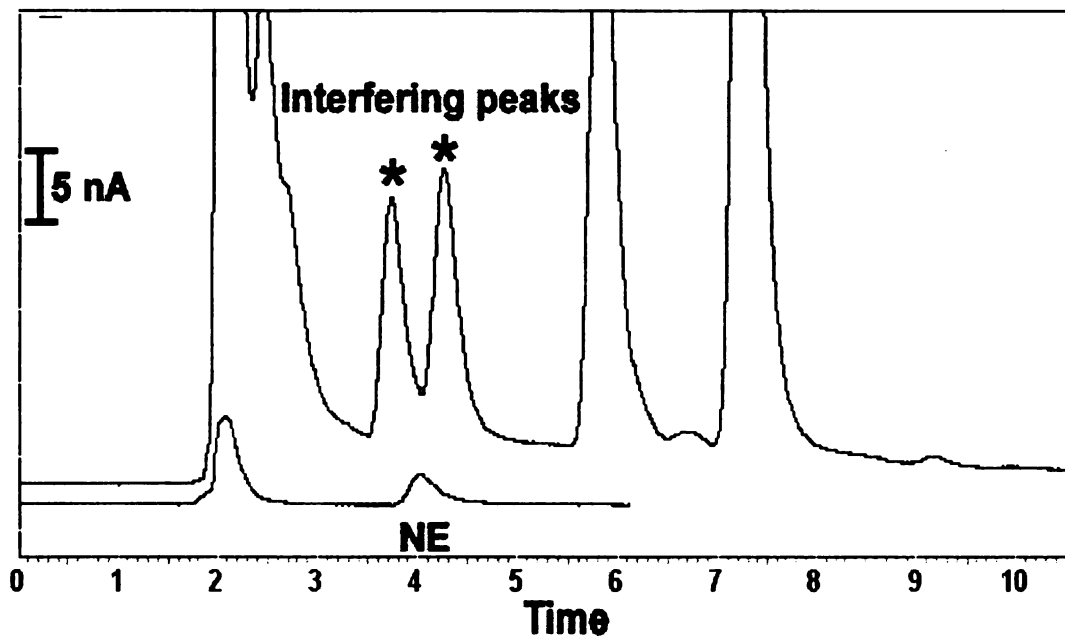


**Figure 4.6** – A chromatogram for a direct injection of the filtered supernatant from a left ventricle sample (upper trace) and a 1  $\mu\text{M}$  NE standard solution (lower trace). The detection electrode was BND.  $E_{\text{det}} = 950 \text{ mV}$  (vs. Ag/AgCl). Flow rate = 1 mL/min. Injection volume = 20  $\mu\text{L}$ . Mobile phase = 50 mM ammonium formate buffer (pH 3).

There are a multitude of methods for extracting biologically important neurogenic amines. Depending on the separation and detection method, one extraction procedure may be more suitable than another. Methods for extracting neurogenic amines range from simple filtration, to liquid-liquid extraction schemes, to many variations of alumina and solid-phase extraction (SPE).<sup>[64, 84]</sup> The extraction procedure selected for use in this work was SPE.

SPE has advantages over other extraction methods, including high recovery for target analytes, good selectivity, and good extraction reproducibility.

SPE is less laborious than either alumina or liquid-liquid extraction. [22, 85] Alumina extraction typically affords a lower yield (NE recovery = 70 – 85 %<sup>[81]</sup>) than SPE but provides greater preconcentration, which is a necessity if the target analyte is present at a very low concentration (i.e., plasma).<sup>[20]</sup> Many different types of SPE cartridges are commercially available and several of these have been used for the analysis of catecholamines in biological fluids, such as blood plasma and urine.<sup>[2, 20, 85, 86]</sup>

The SPE cartridge selected for this work was an Oasis MCX (30 mg / 1 mL). It is a mixed-mode cation-exchange resin on a polymeric support. It is a novel sorbent that enables the selective extraction of basic molecules from complex matrices with dual modes of interaction. The sulfonate groups serve as cationic exchange sites while the aromatic groups provide typical reversed-phase,  $\pi$ - $\pi$  interaction. An illustration of the MCX support material structure and its sites of interaction is presented in Figure 4.7. The MCX cartridge is reported to be stable over a pH range from 0 to 14, which makes it quite versatile for extractions under basic or acidic conditions.

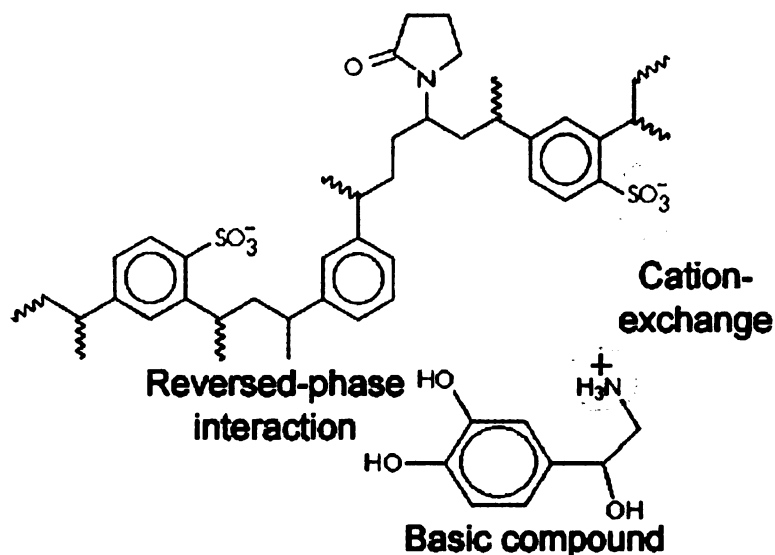


**Figure 4.7.** The molecular structure of the Oasis MCX polymeric sorbent and interaction sites.

The procedure developed was a modified one reported by the manufacturer for catecholamine analysis. The extraction scheme is described in the following paragraphs and is summarized in Table 4.8. The first step was pre-conditioning of the SPE column. This was accomplished by passing 1 mL of methanol followed by two 1 mL volumes of purified, deionized water (18 M $\Omega$ ). The cartridge was then ready for loading of the sample (see section 4.2). A volume (0.5 - 1.0 mL) of the supernatant was loaded along with 500  $\mu$ L of pure water to dilute the sample. During loading, NE, as well as any other protonated species, are retained on the column by a combination of cation-exchange and hydrophobic interactions.

**Table 4.8.** SPE method for the extraction of NE from tissue.

SPE Step	Purpose	Solution
[1.] Conditioning	activation of column	1 mL methanol / 2 mL DI H <sub>2</sub> O
[2.] Loading	analyte retention	0.7 - 1 mL sample + 0.5 mL DI H <sub>2</sub> O
[3.] Washing	removal of interferents	2 mL 0.1 M HCl / 1 mL MeOH
[4.] Eluting	analyte elution	0.7 - 1 mL 250 mM boric acid / 1 M KOH [pH 8.8]

The column was then washed with 2 mL of 0.1 M HCl followed by 1 mL of methanol. The washing step elutes potential interferents and cleans-up the sample. The HCl serves to protonate the amine group on NE and this positively charged functionality interacts with the sulfonate groups on the polymer which 'locks' NE onto the sorbent by electrostatic forces. The methanol elutes polar molecules retained by hydrophobic interaction. The cartridge was then dried by application of a slight vacuum (approximately 400 mm Hg) for 6 min.

The final step in the process was to elute the NE off the stationary phase. Elution was carried out by adding 0.5 – 0.1 mL of 250 mM borate buffer (pH adjusted to 8.8 with 1 M KOH) equal to the initial sample volume. Other reported SPE extraction procedures have used 5% ammonium hydroxide (30%) with methanol and 0.01 EDTA. However, borate buffer was ultimately selected for this work due to the greater yield for NE and because of the large peak attributed to EDTA, which obscured NE determination. The basic solution serves to

deprotonate NE by forming a complex with borate, thus enabling its elution from the stationary phase. Other compounds could potentially be eluted during this step. A quick application of vacuum was used to re-wet the sorbent after drying in the previous step. Once wetted, the solution is left to pass through the cartridge unaided. Once all of the solution passed through, vacuum was applied to pull the remaining solution from the SPE column. The eluate was collected for HPLC analysis.

The first task in the method development was to determine the extraction yield for NE. To do this, the recoveries of NE and EP were calculated. Standard NE solutions were prepared and were subjected to PCA treatment followed by SPE extraction to determine the percent NE recovered. The eluent used for this study was borate buffer (pH 8.8), which was a slight modification to the Waters generic procedure. The recoveries of NE and EP with this eluent were  $95.1 \pm 5.6$  % and  $70.4 \pm 4.5$  % ( $n = 6$ ), respectively. An exceptional recovery for NE was achieved and the ability to extract EP was demonstrated with this SPE procedure.

#### 4.6 HPLC-EC Analysis of Tissue Extracts

Prior to injection, the detection electrode was equilibrated in the mobile phase until a stable background was observed. A series of  $1\mu\text{M}$  NE standards ( $20\ \mu\text{L}$ ) were then injected to verify the analyte retention and electrode response.

A minimum of three injections of a 1  $\mu$ M NE standard was run before tissue extracts each day to validate the response sensitivity and stability of the system.

After the tissue extracts were run, several injections of an NE standard were again made in order to verify retention time and electrode response stability. The peak for NE standard was recorded before and after a series of tissue measurements. When measurements were completed, the column was flushed with 100% acetonitrile for 30 min until the system pressure decreased and the column was clear of aqueous mobile phase in order to prevent damage to the column packing material.

#### 4.6-1 Analysis of Various Tissue Extracts

The first tissues prepared and analyzed were taken from DOCA-salt and normotensive rats. The tissues were from small intestine, spleen, liver, kidney (left and right) and heart. Initially, we attempted to verify that the method was applicable to multiple tissue types with similar interfering compounds and background matrices. However, as the analyses were completed, it was determined that certain tissues were more difficult to comprehensively analyze than others.

Several chromatograms for different tissues are shown below. As one can see, different chromatograms are observed for different tissues and certain tissues appear to be cleaner, that is having less interfering peaks, than others.

The liver was found to be the most difficult to analyze due to large unidentified peaks that eluted near the NE peak. The clarity of the supernatants was also observed to vary considerably. For example, after homogenization and SPE, the liver sample was a faint pink color and the kidney was faint orange, whereas the small intestine and ventricle samples were clear.

As seen below, in Figure 4.8, the analysis of liver tissue was difficult because of many interfering peaks and a large apparent number of solutes that elute after 80 min (not shown). An obscured NE peak (denoted by the arrow) can be seen eluting on the front edge of a larger solute zone. The broad zone, shown eluting between 5 and 8 min, took approximately 80 min to elute and interfered with subsequent injections, as shown in Figure 4.8. Spleen and liver samples seem to both have these in common; very late peaks which elute at approximately 80 min. Multiple injections of these samples, in particular, were problematic. Analysis of small intestine was completed in about 25 min and about 10 min for heart tissue; much less than required for liver or spleen. Kidney samples typically took about 30 min due to late broadened peaks.

Figure 4.9 shows example chromatograms of tissue homogenates from the spleen and left atrium. The spleen is from a DOCA rat and the level of NE is very low as can be seen in the chromatogram. The left atrium obtained from a normotensive rat, on the other hand, has a significant level of NE. An explanation for this is DOCA-salt treated animals are typically expected to have low levels of endogenous NE due to the increased plasma levels of NE found circulating. These increases in plasma or extracellular NE could be reflect (i)

increased firing rates, (ii) greater efflux of NE per firing event, (iii) or inhibited reuptake of NE from the synapse which are physiological effects related to essential hypertension.<sup>[4, 87]</sup> Figure 4.10 is a plot showing the concentrations of NE determined for several tissues. The data are numerically displayed in Table 4.9. The data presented represent the tissue samples for which NE was quantifiable. Many more tissue samples were analyzed but separation and quantification were unsuccessful. The concentrations determined for these tissues are in agreement with other reports in literature.<sup>[19, 88]</sup> Worth noting, is the fact that the DOCA-salt and Sham treatments decrease the NE concentration in the spleen. Routine analysis of these tissues would benefit from an additional clean-up step, such as filtration of the centrifugate prior to SPE.

During analysis of the tissue, it was observed that the heart chromatograms had the least amount of interfering peaks and NE was, in most cases, easily distinguished from any adjacent peaks allowing for its quantification. The clean-up procedure that was developed appears to be most effective for heart tissue. Because of this, it was decided to focus on the analysis of heart tissue for the quantification of NE in the animal models.

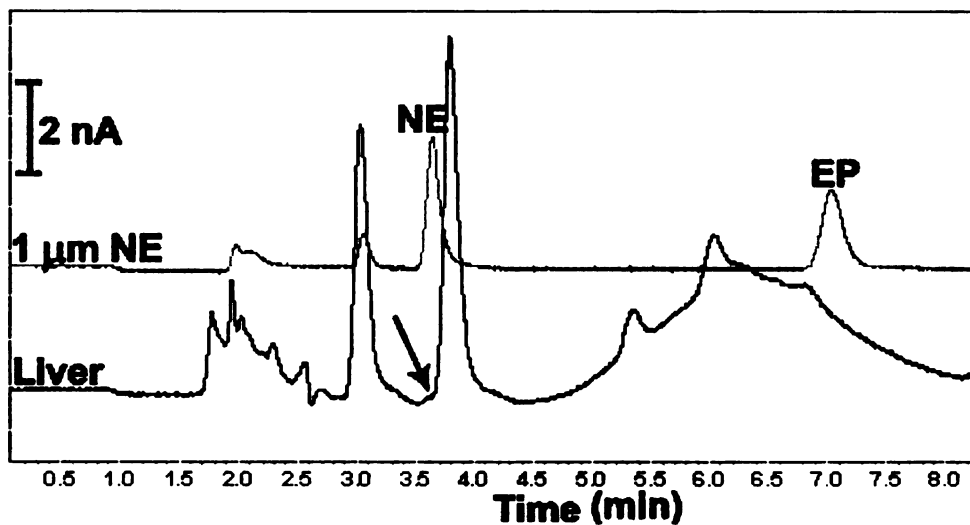


**Figure 4.8.** Chromatogram of liver extract from a DOCA-salt rat. The chromatogram shows a late eluting peak which has caused interference in a subsequent analysis. A small peak, presumably NE can be seen on the edge of the larger peak following. Detection electrode = BND.  $E_{det} = 950$  mV (vs. Ag/AgCl). Flow rate = 1 mL/min. Injection volume = 20  $\mu$ L. Mobile phase = 50 mM ammonium formate buffer (pH3).

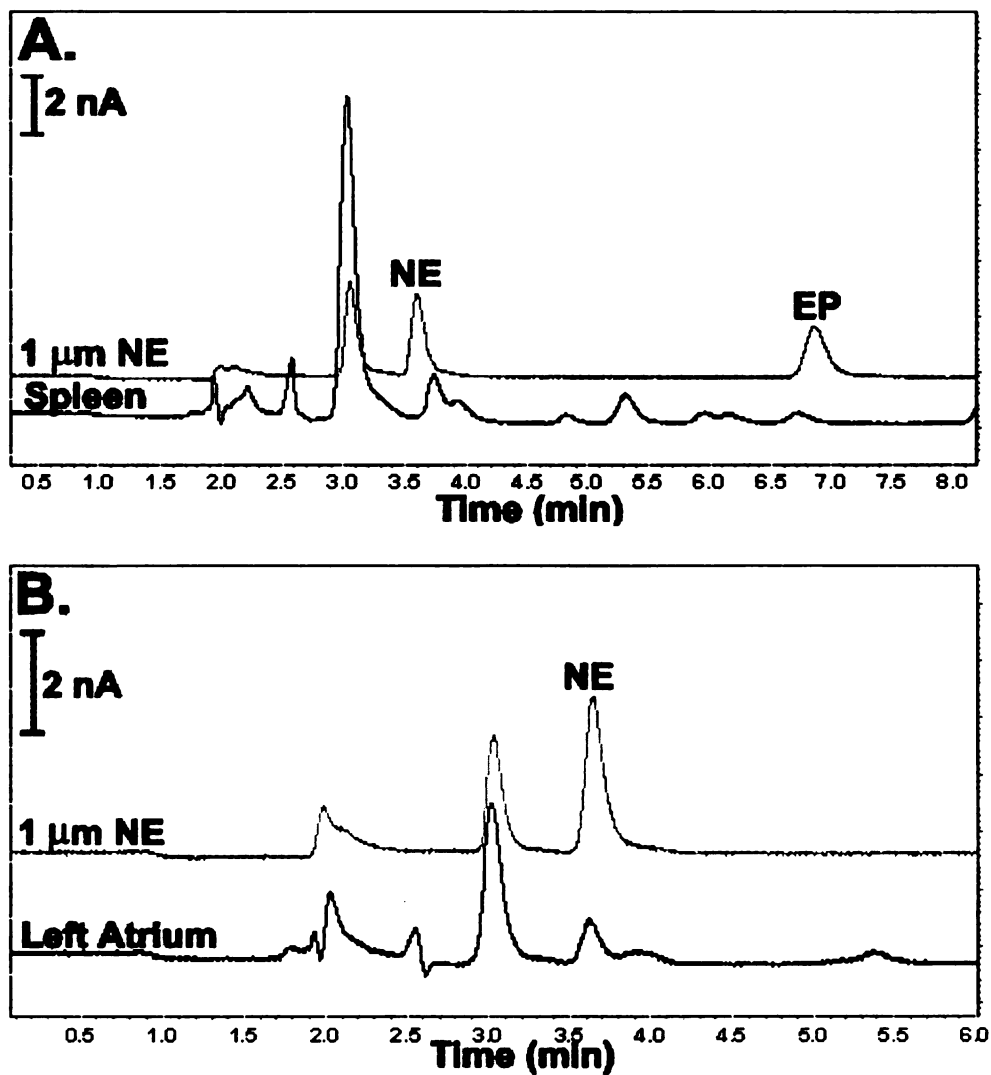


**Figure 4.9** – Chromatograms of (A) spleen extract from a DOCA-salt treated animal and (B) left atrium extract from a normotensive animal. Detection electrode = BND.  $E_{det} = 950$  mV (vs. Ag/AgCl). Flow rate = 1 mL/min. Injection volume = 20  $\mu$ L. Mobile phase = 50 mM ammonium formate buffer (pH3).

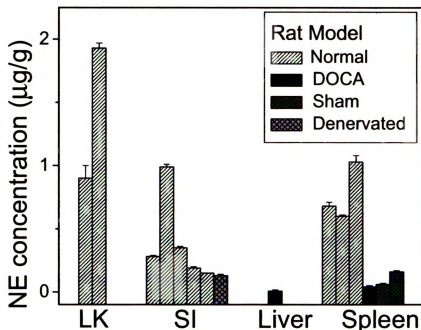


**Figure 4.10.** Concentration of NE found in the tissues from different normotensive, Sham, and DOCA-salt rats. The concentrations were determined by HPLC-EC with BND. LK = left kidney, SI = small intestine.

**Table 4.9.** Concentrations of NE found in the tissues from different normotensive, Sham, and DOCA-salt rats. All concentration values presented as µg NE/g tissue.

	Normal	Sham	DOCA	Denervated
Small Intestine	0.28 ± 0.01 0.99 ± 0.03 0.35 ± 0.01 0.19 ± 0.01 0.15 ± 0.01			0.13 ± 0.01 Below LOD
Left Kidney	0.91 ± 0.10 1.93 ± 0.04			
Liver			0.007 ± 0.01	
Spleen	0.69 ± 0.03 0.60 ± 0.01 1.04 ± 0.05 0.99 ± 0.03	0.16 ± 0.01 0.06 ± 0.01	0.04 ± 0.01	

#### 4.6-2 Analysis of heart tissue and comparison of NE levels in normotensive, Sham, DOCA-salt, and 6-OHDA denervated rats

It was observed that the chromatograms for heart tissue were the cleanest of any tissue type analyzed in terms of the number and intensity of interfering peaks. The separation was complete in about 10 min. NE analysis in different chambers of the heart was conducted to look for regional differences: left and right atria and ventricles and the ventricular septal wall. This study served as a preliminary comparison of the differences of tissue levels of NE found throughout the various rat models. Two rats were analyzed per model type resulting in the analysis of 40 sectionalized chambers. The individual numerical results can be seen in Table 4.10 presented at the end of this chapter.

For all heart tissue analyses NE was quantified by the standard addition method. Standard addition is an accepted method for quantification of a species present in a complex matrix. This method involves adding a known volume and concentration of a standard to the sample and quantifying the amount of unknown analyte by way of a standard addition equation.<sup>[89, 90]</sup> A series of chromatograms for a right ventricle extract from a DOCA-salt rat before and after several standard additions of NE are presented in figure 4.11. Clearly there is no peak deformation or retention time shift after addition of the standard.

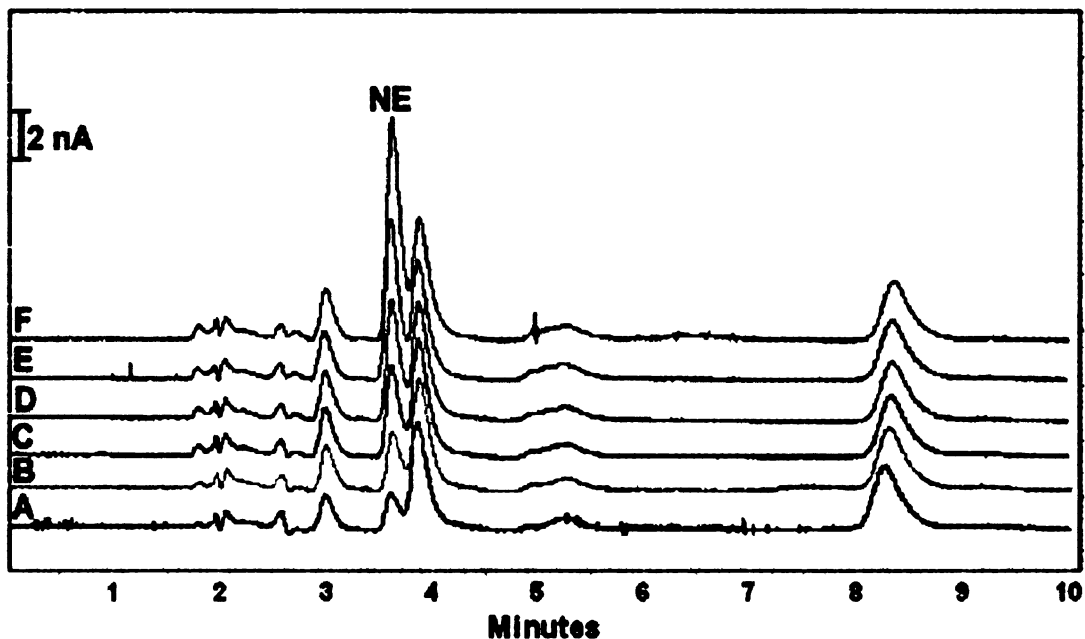


**Figure 4.11.** Chromatograms of a right ventricle extract from a DOCA-salt rat before (A) and after 0.5  $\mu\text{L}$  spikes of a 100  $\mu\text{M}$  NE stock solution (B-F). stacked accordingly. The detection electrode was BND.  $E_{\text{det}} = 950 \text{ mV}$  (vs. Ag/AgCl). Flow rate = 1 mL/min. Injection volume = 20  $\mu\text{L}$ . Mobile phase = 50 mM ammonium formate buffer (pH3).

As depicted in Figure 4.12, it can be seen that the atria have the highest NE level in all of the rat models studied. It can also be observed that 6-OHDA denervation is apparently not as effective for atria, particularly the right atria, as other heart sections. The concentrations of NE in the LV, RV and VSW after treatment with neurotoxin are at or below the LOD. This particular trend has been documented previously, in a similar study where the tissues, namely, heart atria, do not become denervated to the degree of other heart tissue as determined by tissue NE levels.<sup>[78, 91]</sup> In Bentley's study, it was observed that the atria were more resistant to the effects of 6-OHDA, and that the right atrium was

even more resistant than the left atrium. The ventricles were determined to be the most effected by the sympathectomy. However, Bentley used guinea pigs for his research unlike our studies.<sup>[18]</sup>

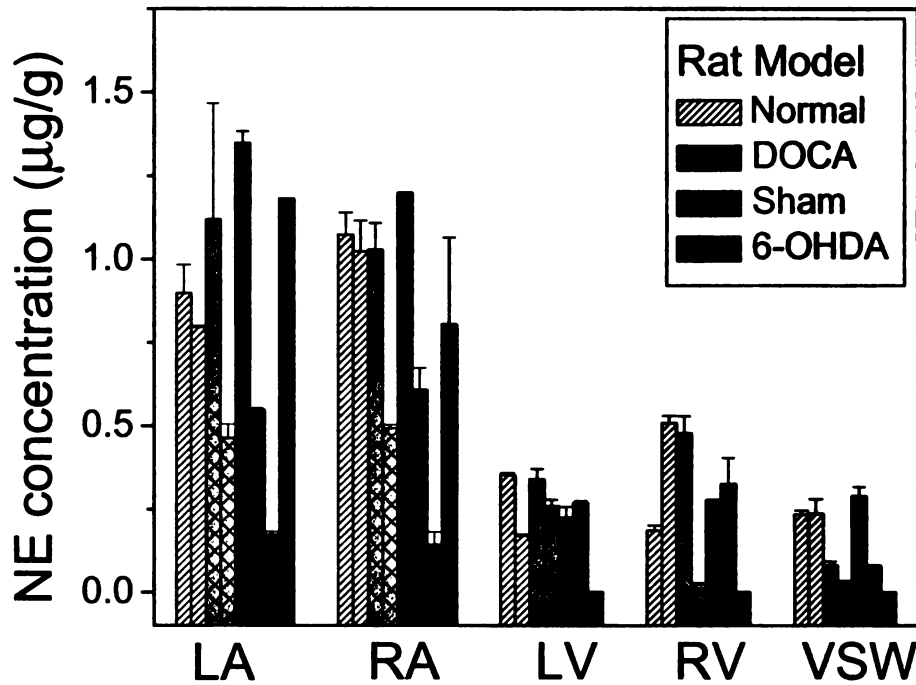


**Figure 4.12** – Concentrations of endogenous NE found in different chambers of the rat heart as determined by HPLC-EC with BND electrode. LA – left atrium; RA – right atrium; LV – left ventricle; RV – right ventricle; VSW – ventricular septal wall.

Norepinephrine concentration, µg/g tissue									
Model	Control		DOCA		Sham		6-OHDA		
#	1	2	1	2	1	2	1	2	
LA	0.90 ± 0.08	0.80 ± 0.01	1.11 ± 0.35	0.46 ± 0.04	1.35 ± 0.04	0.55 ± 0.01	0.17 ± 0.01	1.18 ± 0.01	
RA	1.07 ± 0.07	1.02 ± 0.09	1.03 ± 0.08	0.49 ± 0.01	1.20 ± 0.01	0.61 ± 0.07	0.14 ± 0.04	0.81 ± 0.26	
LV	0.35 ± 0.01	0.17 ± 0.01	0.34 ± 0.03	0.26 ± 0.02	0.22 ± 0.03	0.27 ± 0.01	Below LOD	---	
RV	0.19 ± 0.02	0.51 ± 0.02	0.48 ± 0.05	0.03 ± 0.03	0.28 ± 0.01	0.33 ± 0.08	Below LOD	---	
VSW	0.23 ± 0.01	0.24 ± 0.04	0.03 ± 0.01	0.08 ± 0.01	0.29 ± 0.03	0.08 ± 0.01	Below LOD	---	

**Table 4.10.** Concentrations of NE, determined by HPLC-EC with a BND electrode, in the different chambers of the rat heart from normotensive, Sham, DOCA-salt, and 6-OHDA animals.

In this study, 6-OHDA eliminated any detectable level of NE in both right and left ventricle and the ventricular septal wall. The overall concentrations of NE for heart tissue are similar to concentrations found reported throughout literature, however determination of NE all of the separated chambers is not described fully.<sup>[18, 19, 63, 88, 92]</sup> Further validation of this HPLC-EC method was carried out by two additional methods, capillary electrophoresis (CE) as well as HPLC-CD in a recently submitted paper authored by Dr. Veronika Quaiserova-Mocko and Dr. Martin Novotny.<sup>[93]</sup> The study compares the results of tissue analysis by the three methods and the figures of merit for each instrumental analysis, similar concentrations of NE are found by both CE-EC and HPLC-EC as well as by HPLC-CD.

It can also be noted that there is not a significant difference of NE found in DOCA-salt treated heart tissue compared with that of Sham or normotensive tissue for all of the heart tissue. This is a trend that is unexpected. The level of tissue NE in DOCA-salt treated animals was expected to be lesser than the normotensive and sham treated animal. The sham treated rats only undergo kidney removal; whereas the DOCA treated rats are implanted with a DOCA tablet and given a high-salt diet for several weeks which results in a hypertensive blood pressure (detailed DOCA-salt treatment is discussed in Chapter 2). A decrease in tissue NE levels is thought to be an effect of the excess neuronal release of NE from steady-state stores resulting in increased levels of NE in blood which is associated with hypertension.<sup>[94]</sup>

There is not enough animal data for a full conclusion to yet be drawn. The normotensive data certainly provide a baseline comparison point. These studies have also demonstrated the sample preparation protocol and the separation method are viable for tissue analyses.

#### 4.7 Electrode Response Stability

The electrode response stability is an important property for bioanalysis by HPLC-EC. The response stability of BND evaluated over multiple days of use was RSD = 6.7 %. A plot of the detector signal (oxidation current) versus use time is shown in Figure 4.13. The data were collected using one electrode over the course of several weeks without removing it from the flow cell and without any vigorous cleaning. The only cleaning that was applied was a flushing with HPLC-grade acetonitrile, which was also used to purge the analytical column of any mobile phase after a series of tissue injections. The data below clearly indicate that the BND response is stable over weeks of continuous use (hundreds of tissue injections). The data show that the electrode is useful for the analysis of biological tissue with little or no daily maintenance required to obtain the maximum analytical signal.

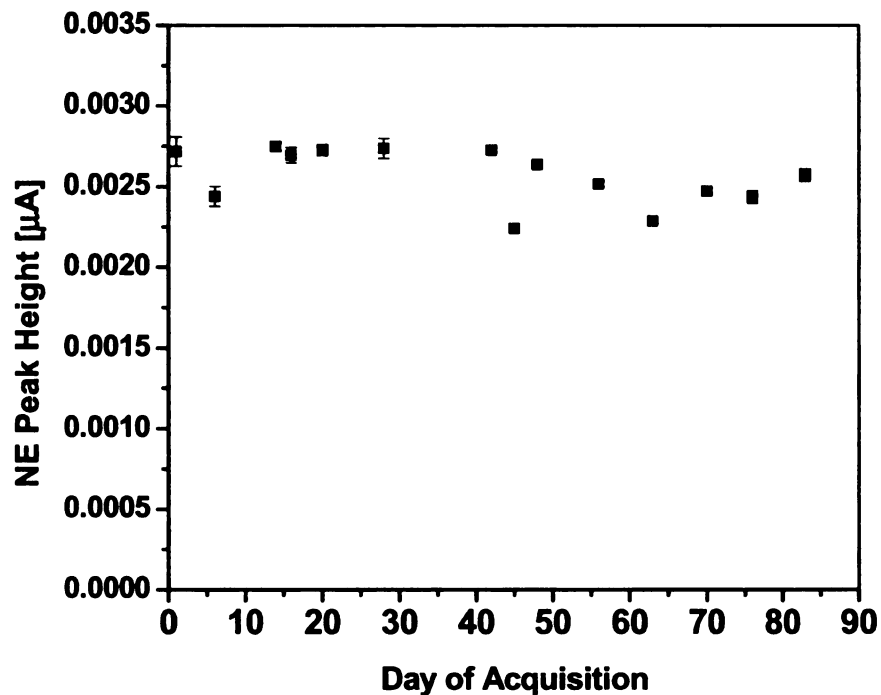


**Figure 4.13.** BND response stability for NE recorded over an 83 day period of use (hundreds of injections). Injections of 1  $\mu\text{M}$  NE standard were made using a single electrode with no maintenance.  $E_{\text{det}} = 950 \text{ mV}$  (vs. Ag/AgCl). Flow rate = 1 mL/min. Injection volume = 20  $\mu\text{L}$ . Mobile phase = 50 mM ammonium formate buffer (pH3). Each point represents the average of 3 separate injections.

## Chapter 5

### Summary of Results and Conclusions

#### 5.1 Conclusions

This body of work demonstrates the applicability and versatility of boron-doped diamond electrodes for the detection of catecholamines in several tissue types. Amperometric detection using glassy carbon has also been reported for tissue analyses like those described in this body of work. Although glassy carbon boasts an increased sensitivity with LOQ's in the low pg range<sup>[2, 85]</sup> (compared to the BND LOQ = 250 pg), this electrode is known for its frequently required maintenance for reactivation which makes it a less attractive mode of detection.<sup>[22, 67, 69]</sup> The BND provided adequate sensitivity for the analysis of rat tissue as demonstrated by this work.

Separation and detection of 7 analytes were performed by our RP-HPLC-EC system. Furthermore, it was demonstrated as a viable method for the separation and detection of biological levels of NE on boron-doped diamond thin-films. The BND boasts analytical response-signal stability over a period of greater than 80 days (RSD = 6.7%). The stability of this electrode proves

beneficial for use in flow-cell environments where repeated disassembling and reassembly for electrode reactivation and/or changing can cause variance in analytical measurements and time consumption. Chronocoulometric studies revealed no evidence of adsorption of NE on either BND or BMD compared with GC which exhibited apparent adsorption of 21 pmol/cm<sup>2</sup>. Semiintegral analysis of the anodic peak obtained from cyclic voltammograms of NE in both pH 2 and 7.2 also verified the lack of adsorption at the BDD and adsorption on GC.

Tissue clean-up and extraction via SPE is another method benefit. SPE has a simple column preparation and extraction procedure when compared with other extraction techniques such as the common alumina extraction used for biological sample clean-up. SPE reproducibly provides a greater sample extraction yield than alumina for determination of NE, as described in chapter 4. The use of a SPE manifold can increase the sample throughput, in our case; up to 12 samples could be extracted simultaneously.

This method also benefits from the use of a simple RP-HPLC mobile phase composition. The ammonium formate buffer used during this study provided a sufficient, reproducible separation requiring no ion-pairing agents or organic solvents as is commonly the case in catecholamine RP-HPLC analysis. The use of an isocratic mobile phase system decreases preparation time and solvent consumption. This buffer also provided ample separation conditions for 6 catecholamines and their metabolites in a period of <12 minutes.

This method provided an efficient means of routinely cleaning and determining NE found within heart tissue in rats. The data was found to

correspond well with previously published values for NE detected in heart tissue (total heart analysis). The concentrations of NE were determined for 3 separate left ventricle, spleen and small intestine samples by this method as well as HPLC with coulometric detection (HPLC-CD) and capillary electrophoresis with electrochemical detection (CE-EC). All of the values were comparable and can be found in a paper recently submitted for publication. The separation of tissue extracts was completed for the determination of NE in ~10 minutes with a relatively clean chromatogram. A drawback of the method is currently only NE can be detected in tissue extracts and the extracted tissue samples have to result in a clean chromatogram. Heart tissue was determined to be the only tissue able to be routinely analyzed. Small intestine was quantifiable, but occasionally a peak would be present in the chromatogram which would obscure the detection of NE. The kidney, spleen, and liver were less easily analyzed due to chromatograms with many interfering peaks; one way to overcome this would be another cleaning step before analysis.

The separation conditions were optimized for many catecholamines and metabolites yet only NE, verified by retention time, is present in the chromatograms of tissue extracts. Although the SPE procedure was determined to have a 70 % recovery for EP, it is not observed in any extracts. It may be possible that EP is present in heart tissue but at lower levels than NE which could be below the LOQ for this system therefore making detection by BND difficult. With a greater sensitivity or using a form of sample preconcentration, EP may in fact be detected and quantitated by this method.

## References

1. T. Yoshitake, J. Kehr, K. Todoroki, H. Nohta, and M. Yamaguchi, *Biomedical Chromatography* 20:267 (2006).
2. C. Sabbioni, M. A. Saracino, R. Mandrioli, S. Pinzauti, S. Furlanetto, G. Gerra, and M. A. Raggi, *Journal of Chromatography A* 1032:65 (2004).
3. M. Luo, M. C. Hess, G. D. Fink, L. K. Olson, J. Rogers, D. L. Kreulin, X. Dai, and J. J. Galligan, *Autonomic Neuroscience: Basic and Clinical* 104:47 (2003).
4. J. Park, V. Quaiserova-Mocko, K. Peckova, J. J. Galligan, G. D. Fink, and G. M. Swain, *Diamond and Related Materials* 15:761 (2006).
5. V. L. Burt, J. A. Cutler, E. J. Roccella, P. Sorlie, and J. Hughes, Vol. 2006, American Heart Association, 2004.
6. G. Pimienta, in The Electrochemical Oxidation and Amperometric Detection of Catechols and Catecholamines at Boron-Doped Diamond Thin-Film Electrodes, *Natural Sciences*, Michigan State University, East Lansing, 2004, p. 82.
7. G. W. Muna, N. Tasheva, and G. M. Swain, *Environ. Sci. Technol.* 38:3674 (2004).
8. Y. Song and G. M. Swain, *Anal. Chem.* (2006).
9. M. Hupert, A. Muck, J. Wang, J. Stotter, Z. Cvackova, S. Haymond, Y. Show, and G. M. Swain, *Diamond and Related Materials* 12:1940 (2003).
10. M. C. Granger, J. Xu, J. W. Strojek, and G. M. Swain, *Anal. Chim. Acta* 397:145 (1999).
11. Y. Show, M. Witek, P. Sonthalia, and G. M. Swain, *Chem. Mater.* 15:879 (2003).
12. J. Park, J. J. Galligan, G. D. Fink, and G. M. Swain, *Anal. Chem.* (2006).
13. J. Cvacka, V. Quaiserova-Mocko, J. Park, Y. Show, A. Muck, and G. M. Swain, *Anal. Chem.* 75:2678 (2003).
14. P. Chen and R. L. McCreery, *Anal. Chem.* 68:3958 (1996).
15. J. Asmussen, D. K. Reinhard, and A. Asmussen, Diamond Thin Films, Marcel Dekker, New York, 2002.

16. A. E. Fischer, Y. Show, and G. M. Swain, *Anal. Chem.* 76:2553 (2004).
17. S. Jolley, M. Koppang, T. Jackson, and G. M. Swain, *Anal. Chem.* 69:4099 (1997).
18. J. A. Bentley, S. Shibata, and J. B. Cheng, *Medical Biology* 53:129 (1976).
19. M. Kawamura, J. P. Schwartz, T. Nomura, I. J. Kopin, D. S. Goldstein, T. Huynh, D. R. Hooper, J. Harvey-White, and G. Eisenhoffer, *Neurochem. Res.* 24:25 (1999).
20. M. A. Raggi, C. Sabbioni, G. Casamenti, G. Gerra, N. Calonghi, and L. Masotti, *Journal of Chromatography B* 730:201 (1999).
21. C.T. Duda, P.T. Kissinger, in Methods in Neurotransmitter and Neuropeptide Research, Part I, Vol. 11 (S.H. Parvez, M. Naoi, T. Nagatsu, S. Parvez, ed.), Elsevier, New York, 1993.
22. J. D. Chi and M. F. Odontiadis, *Journal of Chromatography B* 731:361 (1999).
23. J. Bergquist, A. Sciubisz, A. Kaczor, and J. Silberring, *Journal of Neuroscience Methods* 113:1 (2002).
24. A. Sanchez, E. A. Toledo-Pinto, M. L. Menezes, and O. C. M. Pereira, *Pharmacol. Res.* 50:481 (2004).
25. P. T. Kissinger, C. Refshauge, R. Dreiling, and R. N. Adams, *Anal. Lett.* 6:465 (1973).
26. K. Stulik and V. Pacakova, In Quantitative Analysis of Catecholamines and Related Compounds., John Wiley and Sons, New York, 1986.
27. M. C. Granger, M. Witek, J. Xu, J. Wang, M. Hupert, A. Hanks, M. D. Koppang, J. E. Butler, G. Lucazeau, M. Mermoux, J. W. Strojek, and G. M. Swain, *Anal. Chem.* 72:3793 (2000).
28. S. Ranganathan, T. Kuo, and R. L. McCreery, *Anal. Chem.* 71:3574 (1999).
29. H. B. Martin, A. Argolita, U. Landau, A. B. Anderson, and J. C. Angus, *J. Electrochem. Soc.* 143:L133 (1996).
30. A. J. Bard and L. R. Faulkner, Electrochemical Methods: Fundamentals and Applications, Wiley, Hoboken, 2001.
31. J. A. Bennett, J. Wang, Y. Show, and G. M. Swain, *J. Electrochem. Soc.* 151:E306 (2004).

32. M. D. Hawley, 1984, p. 463.
33. M. D. Hawley, S. V. Tatawawadi, S. Piekarski, and R. N. Adams, *J. Am. Chem. Soc.* 89:447 (1967).
34. J. Li and B. M. Christensen, *Journal of Electroanalytical Chemistry* 375:219 (1994).
35. R. N. Adams, *J. Pharm. Sci.* 58:1171 (1969).
36. G. M. Robinson, E. I. Iwuoha, and M. R. Smyth, *Electrochim. Acta* 43:3489 (1998).
37. W. H. Harrison, W. W. Whisler, and B. J. Hill, *Biochemistry* 7:3089 (1968).
38. A. W. Sternson, R. L. McCreery, B. Feinberg, and R. N. Adams, *Electroanalytical Chemistry and Interfacial Electrochemistry* 46:313 (1973).
39. P. T. Kissinger and W. R. Heineman, *Laboratory Techniques in Electroanalytical Chemistry*, Marcel Dekker, Inc, New York, 1996.
40. J. Zen, A. S. Kumar, and J. Chen, *Electroanalysis* 13:457 (2001).
41. A. Brun and R. Rosset, *Electroanalytical Chemistry and Interfacial Electrochemistry* 49:287 (1974).
42. H. Zhao, Y. Zhang, and Z. Yuan, *Electroanalysis* 14:445 (2002).
43. G. Gerhardt and R. N. Adams, *Anal. Chem.* 54:2618 (1982).
44. W. Chen, X. Lin, H. Luo, and L. Huang, *Electroanalysis* 17:941 (2004).
45. J. Wang, M. Li, Z. Shi, N. Li, and Z. Gu, *Electroanalysis* 14:225 (2002).
46. K. T. Kawagoe, P. A. Garris, and R. M. Wightman, *Journal of Electroanalytical Chemistry* 359:193 (1993).
47. J. Park, J. J. Galligan, G. D. Fink, and G. M. Swain, *Anal. Chem.* 78:6756 (2006).
48. S. H. DuVall and R. L. McCreery, *J. Am. Chem. Soc.* 122:6759 (2000).
49. S. H. DuVall and R. L. McCreery, *Anal. Chem.* 71:4594 (1999).
50. J. Xu, Q. Chen, and G. M. Swain, *Anal. Chem.* 70:3146 (1998).
51. A. W. Bott and W. R. Heineman, *Current Separations* 20:121 (2004).

52. M. S. Freund and A. Brajter-Toth, *The Journal of Physical Chemistry* 96:9400 (1992).
53. R. Bowling and R. L. McCreery, *Anal. Chem.* 60:605 (1988).
54. J. N. Stuart, A. B. Hummon, and J. V. Sweedler, *Anal. Chem.* 76:120A (2004).
55. G. Eisenhoffer, I. J. Kopin, and D. S. Goldstein, *Pharmacological Reviews* 56:331 (2004).
56. H. Blumenfeld, *Neuroanatomy Through Clinical Cases*, Sinauer Associates, Sunderland, 2002.
57. S. H. Parvez, M. Naoi, T. Nagatsu, and S. Parvez, *Methods in Neurotransmitters and Neuropeptide Research*, Elsevier, Amsterdam, 1993.
58. Supelco, 2003, p. 1.
59. H. Chang and E. S. Yeung, *Anal. Chem.* 67:1079 (1995).
60. X. Zhu, P. N. Shaw, and D. A. Barrett, *Anal. Chim. Acta* 478:259 (2003).
61. G. A. Scratchley, A. N. Masoud, S. J. Stohs, and D. W. Wingard, *Journal of Chromatography* 169:313 (1979).
62. M. A. Peat and J. W. Gibb, *Anal. Biochem.* 128:275 (1983).
63. M. Yoshiura, T. Iwamoto, and K. Iriyama, *Jikeikai Medical Journal* 31:169 (1984).
64. A. T. Wood and M. R. Hall, *Journal of Chromatography B* 744:221 (2000).
65. I. Molnar, *Chromatographia* 62:S7 (2005).
66. D. S. Chapin, K. J. Lookingland, and K. E. Moore, *Current Separation* 7:68 (1986).
67. E. Sastre, A. Nicolay, B. Bruguerolle, and H. Portugal, *Journal of Chromatography B* 801:205 (2004).
68. G. Cao and T. Hoshino, *Anal. Sci.* 14:835 (1998).
69. Y. Qu, L. Moons, and F. Vandesinde, *Journal of Chromatography B* 704:351 (1997).
70. M. Przybyciel, *LC Column Technology Supplement*:26 (2004).

71. M. Przybyciel, *Liquid Chromatography Gas Chromatography* 23:554 (2005).
72. S. Corona-Avedaño, A. Rojas-Hernández, M. A. Romero-Romo, M. P. Pardavé, and M. T. Ramírez-Silva, *Spectrochim. Acta, Part A* 61:3139 (2005).
73. S. Corona-Avedaño, G. Alarcón-Angeles, A. Rojas-Hernández, M. A. Romero-Romo, and M. T. Ramírez-Silva, *Spectrochim. Acta, Part A* 61:305 (2005).
74. A. E. Sánchez-Rivera, S. Corona-Avedaño, G. Alarcón-Angeles, A. Rojas-Hernández, and M. T. Ramírez-Silva, *Spectrochim. Acta, Part A* 59:3193 (2003).
75. M. S. Chi, J. G. Vander Tuig, C. H. Chi, A. Norman, L. Chapman, and T. Blanks, *Proc. Soc. Exp. Biol. Med.* 215:174 (1996).
76. M. Yoshiura and T. Iwamoto, *Jikeikai Medical Journal* 21:21 (1985).
77. A. Caplea, D. Seachrist, H. DaneShvar, G. Dunphy, and D. Ely, *J. Appl. Physiol.* 92:567 (2002).
78. P. M. Lear and J. R. Prohaska, *Proc. Soc. Exp. Biol. Med.* 215:377 (1997).
79. R. B. Gibbs, D. Edwards, N. Lazar, D. Nelson, and J. Talameh, *J. Neuroendocrinol.* 18:643 (2006).
80. T. A. Durkin, E. J. Caliguri, I. N. Mefford, D. M. Lake, I. A. Macdonald, E. Sundstrom, and G. Jonsson, *Life Sci.* 37:1803 (1985).
81. M. Candito, A. M. Krstulovic, V. Sbirazzuoli, and P. Chambon, *Journal of Chromatography B* 526:194 (1990).
82. J. Park, Y. Show, V. Quaiserova-Mocko, J. J. Galligan, G. D. Fink, and G. M. Swain, *Journal of Electroanalytical Chemistry* 583:56 (2005).
83. P. Kalen, R. E. Strecker, E. Rosengren, and A. Bjorklund, *J. Neurochem.* 51:1422 (1988).
84. F. A. J. Van Der Hoorn, F. Boomsma, A. J. Man In 'T Veld, and M. A. D. H. Schalekamp, *Journal of Chromatography* 487:17 (1989).
85. M. A. Raggi, C. Sabbioni, G. Nicoletta, R. Mandrioli, and G. Gerra, *Journal of Separation Science* 26:1141 (2003).

86. N. Unceta, E. Rodriguez, Z. Gomez de Balugera, C. Sampedro, M. A. Goicolea, S. Barrondo, J. Salles, and R. J. Barrio, *Anal. Chim. Acta* 444:211 (2001).
87. G. A. Crabb, R. J. Head, J. Hempstead, and B. A. Berkowitz, *Clinical and Experimental Hypertension* 2:129 (1980).
88. Q. Chen, Y. Nishida, M. Zhou, H. Murakami, H. Morita, H. Hosomi, and H. Kosaka, *Journal of the Autonomic Nervous System* 71:175 (1998).
89. D. C. Harris, Quantitative Chemical Analysis, W. H. Freeman and Company, New York, 2003.
90. M. Mayer and J. Ruzicka, *Anal. Chem.* 68:3808 (1996).
91. S. Kitano, *Circ. Res.* 46:681 (1980).
92. N. R. Keller, A. Diedrich, M. Appalsamy, S. Tuntrakool, S. Lonce, C. Finney, M. G. Caron, and D. Robertson, *Circulation*:1191 (2004).
93. V. Quaiserova-Mocko, M. Novotny, L. S. Schaeffer, G. D. Fink, and G. M. Swain, Submitted XXX:XX (2006).
94. M. Luo, G. D. Fink, K. J. Lookingland, J. A. Morris, and J. J. Galligan, *American Journal of Physiology - Heart and Circulatory Physiology* 286:1558 (2003).